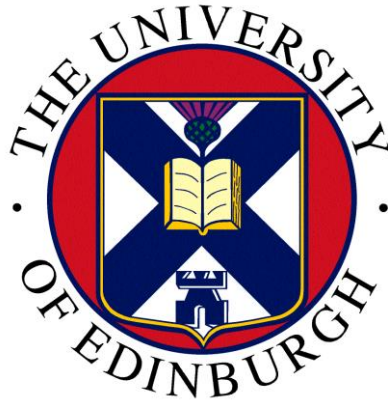


NERC Scientific Facilities and Technology

Ion Microprobe Facility



University of Edinburgh
NERC Ion Microprobe Facility

2019 Annual Science Report

Ion Microprobe Facility
School of Geosciences
Kings Buildings
James Hutton Road
Edinburgh
EH9 3FE

<http://www.ed.ac.uk/geosciences/facilities/ionprobe>

Contents

No.	Authors	Project Title	p.
1	Bamber E.C., M.R. Burton et al.	Understanding basaltic Plinian eruptions	1
2	Becerra-Torres E., E. Melekhova et al.	Characterising mantle wedge chemistry and thermal structure beneath the Colima Graben, Mexico	3
3	Bravenec A. & G. Bromiley	Effect of oxygen fugacity on water partitioning into the early Earth's mantle	5
4	Carter E. J. & B. O'Driscoll	Tracing subducted volatile fluxes through halogen abundances in the leading edge of the mantle wedge	7
5	Cassidy M.	Water saturation and temperature changes affect halogen degassing of shallow magmas	9
6	Clarke E.R & J.C.M. De Hoog	Oxygen isotope constraints on serpentinite dehydration in subduction zones	11
7	Clarke E.R., J.C.M. De Hoog & G. Bromiley	Boron isotope partitioning between fluid and olivine	13
8	Cortés J.A. & E.S. Calder	Volatile degassing styles and the triggering of an eruptive event in an open, persistently degassing volcanic system, Villarrica volcano, Chile	15
9	Crosby J.C., S.A. Gibson et al.	The source and flux of volatiles in off-craton lithospheric mantle	17
10	Georgieva M.N., C.T.S Little et al.	Investigating the fossilisation and nature of sulphur metabolisms within associated fossil vent animals and microbes	19
11	Hastie A.R.	Can drips or delamination generate the Eoarchean continental crust? (pilot study)	21
12	Hutchinson M.C., R.A. Brooker & J.D. Blundy	Trace element partitioning between sulphate phases and silicate melts in arc magmas	23
13	Jackson C.G. & S.A. Gibson	Halogen storage in nominally volatile-free minerals in the sub-cratonic lithospheric mantle	25
14	Lapponi F., I. Troth & J. Craven	Origin of silica in presalt carbonates: insights from ion probe O isotopic analysis	27
15	Mather T.A.	Using S isotope in melt inclusions to understand S cycling through subduction zones (pilot study)	29
16	McCarthy A., J. Ryker & J. Blundy	The effect of rapid crystal-growth on trace element partitioning in plagioclase and clinopyroxene	31
17	McMahon S., J. Parnell & P. Reekie	EMBARGO Sulfur isotope evidence of ancient subsurface life: implications for Mars	33
18	Potts N.J. & G.D. Bromiley	Chlorine Isotope fractionation during degassing of lunar magmas	35
19	Smith V., M. Humphreys et al.	Constraining the volatile history of the Campanian Ignimbrite eruption	37
20	Tabassum N., S.C. Kohn et al.	Investigating the water content of diamond inclusions: analysis of trace element concentration of olivine diamond inclusions and olivine synthesised in equilibrium with saline-rich fluid	39

21	Taracsák Z., M.E. Hartley et al.	Sulfur isotopic evidence for a volatile-enriched recycled component in the Canary Islands mantle source	41
22	Walton C., N. Potts, et al.	Deep volatile cycling and terrestrial thermal evolution (pilot study)	43
23	Walton C., O. Shorttle & M. Anand	Is Early Earth bombardment history recorded in shocked meteorites? (pilot study)	44
24	Waters E., M. Hartley et al.	Trace element compositions of Snæfellsjökull, Oræfajökull and Miðfell volcanic centres, Iceland	45
25	Wieser P. E., H. Lamadrid, et al.	Petrological insights into the volatile budget of the 2018 Kīlauean eruption	47

Understanding Basaltic Plinian Eruptions

E.C. Bamber¹, M.R. Burton¹, M. Polacci¹, M. Hartley¹, G. La Spina¹, M. de' Michieli Vitturi², F. Arzilli¹

¹ Department of Earth and Environmental Sciences, The University of Manchester, Manchester, M13 9PL, UK

² INGV, Sezione di Pisa, Pisa, 56125, Italy

Introduction

Plinian eruptions are amongst the most poorly understood styles of volcanic activity at basaltic systems, yet are the most hazardous. Fragmentation during magma ascent produces a column of hazardous gas and ash erupted at the surface, depositing several km³ of tephra. However, the low viscosity and long relaxation time of basaltic magma should preclude its fragmentation during magma ascent, producing effusive activity and low explosive eruptions [1]. The possibility of a Plinian eruption presents a significant risk to the ever increasing populations living in these areas. However, the mechanisms producing basaltic Plinian eruptions are still strongly debated. We aim to test diverse hypotheses as the cause of basaltic Plinian eruptions at the Las Sierras-Masaya complex, Nicaragua.

In order to test these hypotheses, it is essential to have accurate constraints on the pre-eruptive volatile budget of these eruptions, such as H₂O and CO₂, where their exsolution can influence eruption dynamics. We compare two Plinian eruptions of the Las Sierras-Masaya complex, the Fontana Lapilli (60 ka) and Masaya Triple Layer (2 ka). However, data on the pre-eruptive volatile budget of these eruptions is currently lacking, with only a single measurement for CO₂ for the Fontana Lapilli eruption [2]. We aim to provide the first data constraining the pre-eruptive volatile budget for eruptions of the Las Sierras-Masaya complex, by quantifying H₂O, CO₂, Cl and F in phenocryst-hosted melt inclusions using the SIMS technique. This data will be incorporated into a numerical conduit model, which is able to simulate degassing and crystallisation during ascent and investigate eruption dynamics of basaltic Plinian volcanism.

Methodology

Scoriae of the Fontana Lapilli (FL) and Masaya Triple Layer (MTL) eruptions were collected during a 2018 fieldwork campaign in Nicaragua. Scoriae were mounted in epoxy resin and polished to expose melt inclusions hosted in plagioclase phenocrysts (Fig. 1). H₂O, CO₂, F, Cl and Ce in melt inclusions and matrix glasses were measured using the Cameca IMS 7f-Geo during a session in December 2019. Major element concentrations were measured using the JEOL JXA-8530F FEG electron microprobe at the Photon Science Institute, University of Manchester. Acquired data was then incorporated into the 1D multiphase, steady-state numerical conduit model of La Spina et al., [3] in order to evaluate the relative contributions of different conduit processes to enhanced explosivity.

Results

Complete results are still pending a visit to the facility in April 2020. However, preliminary results from the December 2019 session allow trends to be discerned by comparing the volatile budgets of the FL and MTL eruptions. A larger range in stored H₂O concentration is observed for melt inclusions of the FL eruption (0.91-2.2 wt. %) as opposed to melt inclusions of the MTL eruption (1.06-1.21 wt. %) (Fig. 2a). A higher stored CO₂ concentration is observed for the FL eruption (100-1120 ppm), compared to the MTL eruption (130-300 ppm). FL melt inclusions exhibit a halogen enrichment (Cl = 1680-2370 ppm; F = 950-1190 ppm) relative to MTL melt inclusions (Cl = 1180-1540 ppm; F = 780-1050 ppm) and a greater range in concentration (Fig. 2b).

Discussion and future objectives

Measured H₂O and CO₂ concentrations are consistent with the pre-eruptive condition inferred for the storage reservoir of the Masaya caldera complex, where magma evolution is dominated by plagioclase crystallisation at low pressure and low H₂O concentrations [4].

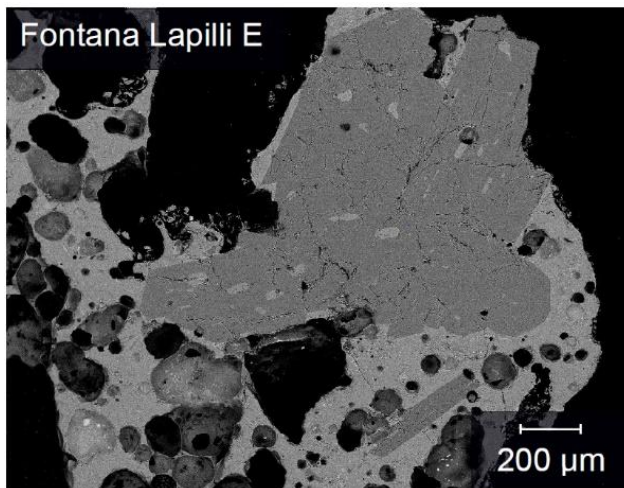
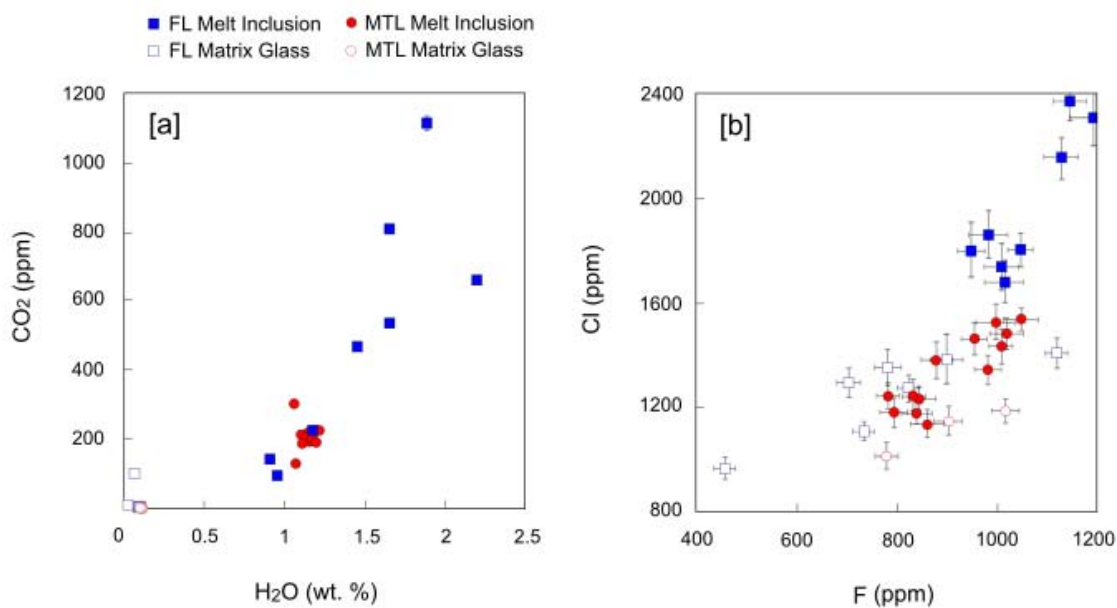


Figure 1. A BSE image of scoria from Plinian phase unit E of the Fontana Lapilli eruption, showing melt inclusions hosted in plagioclase phenocrysts.

Figure 2 (a-b). Volatile and major element compositions of melt inclusions and matrix glasses of the Fontana Lapilli (blue) and Masaya Triple Layer (red) eruptions. (a) H₂O (wt.%) vs CO₂ (ppm). (b) F (ppm) vs Cl (ppm). Error bars not shown are within the size of



Preliminary numerical simulations indicate that this measured volatile budget can satisfy the brittle fragmentation criterion and result in explosive eruption. Higher H₂O and CO₂ concentrations suggest that the FL magma was potentially stored at greater depth. The more evolved composition of the FL magma (SiO₂ 52.7-54.7 wt. %) compared to the MTL (SiO₂ 51-52.6 wt. %) attests to the fact that there may have been an evolution in the magma storage condition at the Las Sierras-Masaya complex through time. Halogen data of the MTL and FL eruptions also yield an interesting comparison. The two eruptions appear to exhibit different trends in terms of the stored halogen concentrations in melt inclusions and their relationship with matrix glasses. A greater degree of variability is observed in the halogen concentrations of FL melt inclusions. The objectives for the remaining acquisition time are to analyse more samples from different units of the eruptions, to constrain the extent of this geochemical variability and its temporal evolution over episodic eruptions with stages of varying explosivity. Comparing the pre-eruptive condition is crucial to investigate potential triggering mechanisms of basaltic Plinian volcanism.

References

- [1] Parfitt E.A. (2004) *Journal of Volcanology and Geothermal Research*, 134, 77-107.
- [2] Wehrmann H. et al. (2011) *Geochemistry Geophysics Geosystems*, 12 (6).
- [3] La Spina G. et al. (2016) *Nature Communications*, 7.
- [4] Walker J.A. et al. (1993) *Journal of Volcanology and Geothermal Research*, 56, 379-400.

Characterising mantle wedge chemistry and thermal structure beneath the Colima Graben, Mexico

E. Becerra-Torres, E. Melekhova, J. Blundy & R. Brooker

School of Earth Sciences, University of Bristol, Bristol BS8 1RJ, UK

Introduction

Primitive arc magmas provide information about the nature and thermal structure of the underlying mantle wedge. In the Colima Graben, Mexico, primitive lavas erupted from cinder cones range from high magnesium calc-alkaline basalts to shoshonitic trachybasalts. This chemical diversity suggests that the sub-arc mantle wedge from which they derive is heterogeneous. To explore the conditions of magma generation in the wedge beneath Colima we used an inverse experimental approach to constrain multiple saturation points on the liquidus surface of a primitive high-K basanite (COM-1). Equilibrium piston-cylinder experiments were carried out between 1.0 and 2.4 GPa under hydrous (1.8 to 3.8 wt% H₂O) and oxidizing ($fO_2 = 0.3$ to 4.5 log units above NNO) conditions.

Results and discussion

COM-1 + 3.8 wt% H₂O is shown to be multiply-saturated with a phlogopite-bearing spinel pyroxenite assemblage (cpx+opx+phl+sp) close to its liquidus at 1.9-2.4 GPa and 1300 °C. In this study we consider an experiment to be multiply saturated if it crystallises at least four mineral phases very close to its liquidus (>95% melt). Experimental mapping of the liquidus surface reveals a multiple saturation point (MSP) where a lherzolitic phase assemblage of ol+cpx+opx+sp+phl coexist (Fig. 1). The topology of the MSP indicates a peritectic of the form cpx+opx+phl+sp=liquid+ol. Four bracketing experiments define the MSP of COM-1 as **1300±10 °C, 1.7±0.1 GPa, ΔNNO = 3.4±0.5 log units, for melt containing 3.6±0.4 wt% H₂O**. The MSP olivine is too forsterite-rich (Fo₉₂₋₉₄) to be in equilibrium with mantle lherzolite, but matches phenocryst core compositions in the natural basanite. Thus, experimental results indicate that COM-1 was produced by incongruent melting of a phlogopite-pyroxenite source, itself the result of metasomatism of mantle wedge by slab-derived fluids. These conditions provide a unique constraint on the thermal structure and chemical composition of the mantle wedge.

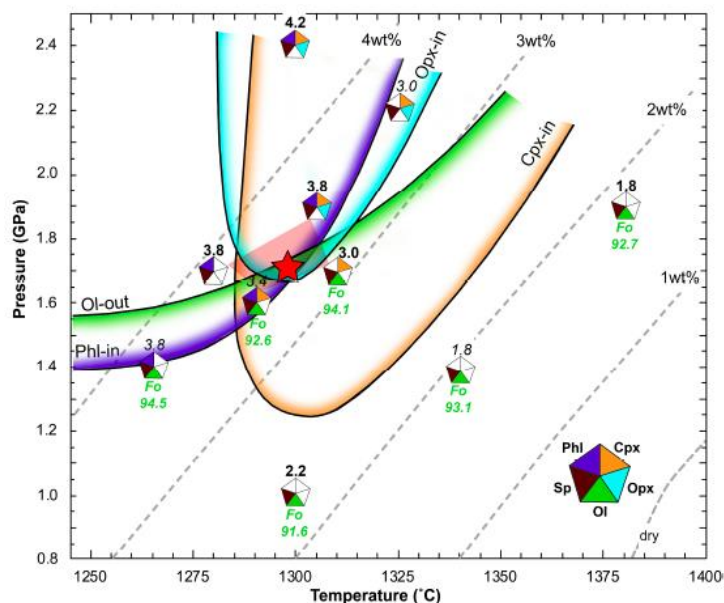


Figure 1. Liquidus surface diagram for bulk composition COM-1. Only experiments containing >95% glass are plotted. Different colours represent stability regions of the key mineral phases in the pentagon key. The olivine composition (as mol% Fo in green) and the melt H₂O content are marked next to each experiment; measured (SIMS) values are shown in bold font and values estimated by mass balance in regular font. Liquidus contours (dashed grey) are labelled with the corresponding H₂O content of the melt; the “dry” liquidus was generated using pMELTS. The pink shaded quadrilateral containing the red star, is defined by the 4 surrounding experiments. These define the peritectic liquidus multiple saturation point (MSP) of COM-1 for Comal Chico primary magma.

Analytical details

Volatile contents of experimental glasses were analysed by secondary ion mass spectrometry (SIMS) at the NERC ion microprobe facility at University of Edinburgh, using a Cameca IMS 7f-Geo instrument with a nominal 10 kV primary beam of $^{16}\text{O}^-$ ions and 5 nA beam current, resulting in a spot size at the sample surface of $\sim 15\ \mu\text{m}$. H_2O and CO_2 were calibrated against synthetic basaltic glass standards containing ≤ 4 wt% H_2O and ≤ 2200 ppm CO_2 . Working curves of $^1\text{H}/^{30}\text{Si}$ vs H_2O and $^{12}\text{C}/^{30}\text{Si}$ vs CO_2 gave straight lines with $R^2 \geq 0.99$ (Fig. 2). High mass resolution eliminates all interference on $^{12}\text{C}^+$ by $^{24}\text{Mg}^{2+}$. In total 25 experimental glasses were analysed for H_2O and CO_2 .

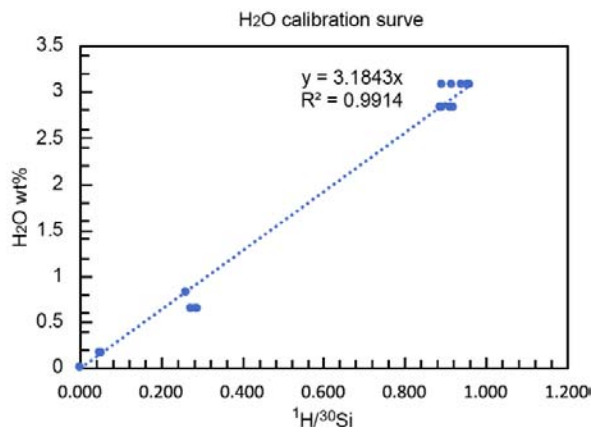


Figure 2. Working curves for SIMS analysis of H_2O in basaltic glass. Abscissa denotes ratios of counts per second for $^1\text{H}^+$ normalized to ^{30}Si .

Effect of oxygen fugacity on water partitioning into the early Earth's mantle

A. Bravenec, G. Bromiley

School of GeoSciences, University of Edinburgh, Edinburgh EH9 3JW, UK

Overview

Water had a fundamental influence on the formation, evolution, and potential for habitability on Earth and other terrestrial bodies. **Incorporation of trace amounts of water in Earth's** interior also exerts a strong influence on key physical and chemical properties, including partial melting, rheology, electrical and thermal conductivity, cation diffusion, phase transition boundaries, and the exchange of water **between Earth's interior and exterior** [1-8]. Interior volatile abundances (primarily H and C) may have **influenced the development of Earth's oceans, atmosphere, and by inference**, the emergence of life. However, the behaviour of water and other volatiles under the more reducing conditions of early planetary interiors and magma oceans remains poorly constrained. Our understanding **'water'** incorporation in mineral/melt structures at high pressures/temperatures is largely based on experiments performed under the relatively oxidising conditions of Earth's upper mantle, where OH⁻ dominates. In more reduced systems **it is likely that speciation of 'water'** is very different. Any change in speciation likely alters the effect of **'water'** on mantle properties and processes, implying that our understanding of reduced planetary systems such as the early Earth is limited.

Here, we aim to constrain H and C budgets of early planetary interiors with their evolving oxidation states, chemical compositions, and thermal histories. The early Martian mantle, lunar mantle, and terrestrial magma ocean experienced highly reducing conditions below the IW redox buffer. Thus, to assess the H storage capacity of planetary mantles, the influence of oxygen fugacity (f_{O_2}) must be constrained. This presents a number of challenges, as it involves performing experiments under H-rich but low f_{O_2} conditions. Following development of a new experimental protocol, we have performed a series of high-pressure/temperature experiments to constrain H incorporation in mineral and melt phases at low f_{O_2} . SIMS and EMPA of run products is used to determine mineral and melt chemistry and H₂O and CO₂ contents. Coupled with the results of IR/Raman spectroscopy (with R. Brooker, U. Bristol) this then allows us to model the behaviour of C and H during early Earth processes, as well as constrain the incorporation of these elements across more reduced bodies in the inner solar system.

Preliminary Results

Our results, using a simplified model system, demonstrate that f_{O_2} exerts a fundamental control on H solubility and partitioning. Both the solubility of H in olivine, and partitioning of H between olivine/melt ($D^{H_{\text{olivine/melt}}}$) are significantly lower under more reducing conditions (Fig. 1). Raman analysis confirms that reducing conditions stabilise formation of H₂ in magmas, especially at higher pressures. An increase in the ratio H₂/H₂+OH⁻ in silicate melt likely drives a decrease in measured H₂O content (i.e. H content) of olivine in which H₂ incorporation is less favourable. This results in systematic decreases in $D^{H_{\text{olivine/melt}}}$. In contrast, we see no evidence for the presence of other reduced H related species such as CH₄, even under highly reduced conditions. This implies that decrease in f_{O_2} drives progressive decrease in C solubility in melt as CO₂ becomes less stable.

In addition to this work we have also determined H and C solubility and speciation (SIMS, Raman and IR analysis) in coexisting olivine/pyroxene/silicate melt in a series of nominally anhydrous, carbon saturated Martian analogue experiments synthesized by Filiberto and co-workers [15-17]. These experiments were conducted in more complex systems under moderately reducing conditions. Comparison of this dataset with our new experimental data, and with wider literature data [e.g. 9-14] is being used to identify complex inter-relationships between **'water' activity, temperature, pressure, f_{O_2}** and bulk composition (as shown in Fig. 2). This will be used to develop comprehensive model of H incorporation and partitioning in reduced systems, and reassess the behaviour and role of H in the early Earth, and in reduced, terrestrial bodies.

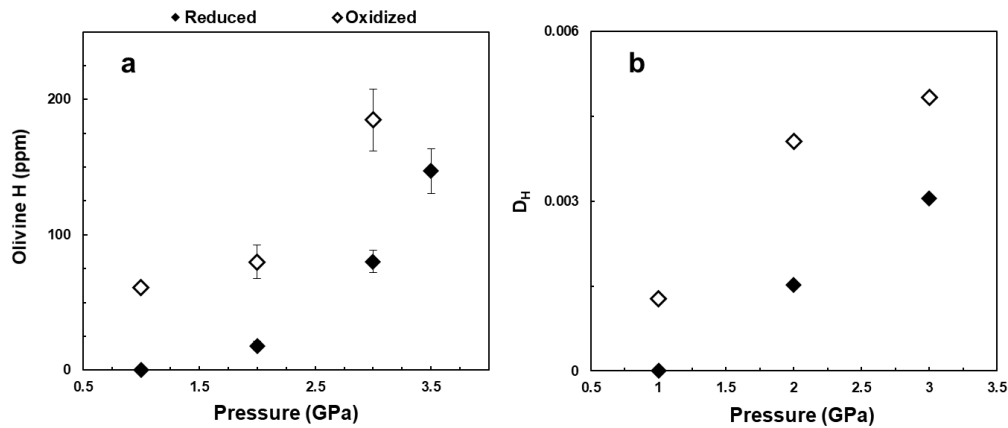


Figure 1. Data subset from ion microprobe analysis of reduced (-IW-5) and oxidized (-NNO) piston-cylinder run products as a function of pressure. a) Hydrogen contents of olivine determined by SIMS, b) hydrogen partitioning coefficient between olivine and coexisting silicate melt.

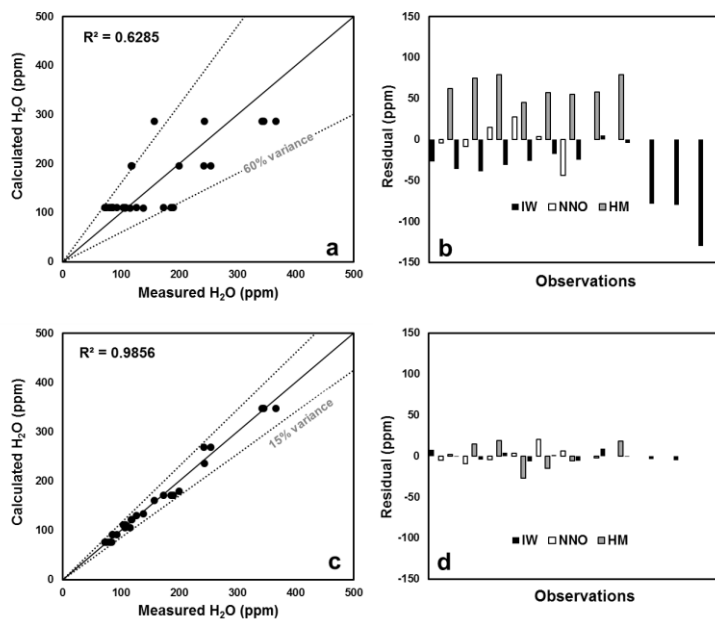


Figure 2. Comparison of measured water solubilities in olivine and solubilities predicted by thermodynamic calculations.

a) Solubility calculated ignoring fO_2 with b) showing the systematic underestimation and overestimation according to redox buffer (IW, NNO, and HM). Both c) and d) show a significantly improved model when accounting for fO_2 . This reanalysis of data from Yang [12] demonstrates the importance of fO_2 in controlling how 'water' would behave during the crystallisation of the Moon and provides an example of future modelling work.

References

- [1] Karato S. (1990) *Nature* 347, 272-273
- [2] Bell D.R. and Rossman G. R. (1992) *Science* 255, 1391-1397
- [3] Wood B.J. (1995) *Science* 268, 74-76
- [4] Ingrin J. and Skogby H. (2000) *Eur. J. Mineral.* 12, 543-570.
- [5] Hirschmann M. (2006) *Annu. Rev. Earth Planet. Sci.* 34, 629-653.
- [6] Keppler H. and Smyth J. R. (2006) *Mineralogical Society of America*, Washington, DC.
- [7] Hirschmann M. and Kohlstedt D. L. (2012) *Phys. Today* 65.
- [8] Peslier et al. (2017) *Space Sci Rev.* DOI: 10.1007/s11214-017-0387-z.
- [9] Grant, K. J. et al. (2007). *Earth Planet. Sci. Lett.* 261, 217-229.
- [10] Gaillard F. et al (2015) *Chem. Geol.* 418, 217-233.
- [11] Gaetani, G.A. et al. (2014) *Contrib. Mineral. Petrol.* 167, 968-910.
- [12] Yang, X. (2016) *Geochim. Cosmochim. Acta* 173, 319-336.
- [13] Tollan P.M.E. et al. (2017) *Progress in Earth and Planetary Science* 4, 14.
- [14] Newcombe, M.E. et al. (2017) *Geochim. Cosmochim. Acta* 200, 330-352.
- [15] Filiberto, J. et al (2008) *MAPS* 43, 1137-1146.
- [16] Filiberto, J. et al (2010) *Geophys. Res. Lett.* 37, L13201.
- [17] Filiberto, J. et al (2010) *MAPS* 45, 1258-1270.

Tracing subducted volatile fluxes through halogen abundances in the leading edge of the mantle wedge

E. J. Carter¹ & B. O'Driscoll¹

¹Department of Earth and Environmental Sciences, University of Manchester,
Oxford Road, Manchester M13 9PL, UK

Background and rationale

Subduction of oceanic lithosphere represents a first-order coupling of the surface and interior of the Earth. The subduction process forms a key part of the geochemical cycles of many volatile elements including carbon and the halogens, with wider implications for global climate and long-term ocean salinity, respectively [1]. Establishing the magnitude of any flux into the deep Earth requires evaluating mass balance between inputs to the subduction system – via altered oceanic lithosphere – and outputs – via slab dehydration and arc volcanism. The magmatic complexities of arc volcanism make quantification of the fluxes associated with dewatering of the slab problematic [2]. In addition, much of the shallow mantle wedge is not sampled by volcanism, **potentially leading to “hidden” outfluxes**. Estimates of volatile fluxes to the mantle are, as a result, highly uncertain. Ophiolites can help to resolve these issues. They comprise oceanic lithosphere tectonically uplifted during plate collisions. Most ophiolites in the geological record have undergone processing above subduction zones during their emplacement and provide evidence for metasomatism of the mantle wedge by percolating melts or fluids [3].

Samples and geological setting

The ~96 Ma Semail Ophiolite, Oman, is the largest known and best studied ophiolite in the world. The basal thrust of the ophiolite tectonically juxtaposes mantle peridotites on top of metasediments and metabasalts, together interpreted as remnants of the shallow parts of a subduction zone. In places, the basal thrust is overlain by mantle peridotites which have undergone complete carbonation to form listvenites – unusual rocks consisting principally of magnesite (MgCO_3) and quartz (SiO_2). It has been suggested that these formed at shallow subduction levels, at temperatures of 100-200°C, through metasomatism by CO_2 -rich fluids derived from the downgoing plate [4]. The basal thrust section has recently been sampled by diamond core drilling, as part of the Oman Drilling Project (International Continental Drilling Program expedition 5057). This unique core affords almost complete preservation across a reaction front between the serpentinite protolith (hydrated peridotite) via progressively **altered “ophicarbonates”** into listvenite (carbonated peridotite). The interval shows a sharp compositional gradient over which external factors such as protolith heterogeneity or later alteration will be minimised and the dominant variation should be due to increasing influence of the carbonating fluid. The principal aim of this project is to test the hypothesis that fluids derived from subducting sediments are the source of CO_2 -rich fluids. If confirmed this would suggest carbonation at the leading edge of the mantle wedge may be a significant and overlooked part of the global carbon cycle. If a component derived from the subducting slab is identified, we further aim to reconstruct the halogen signature of slab fluid(s) to better understand their fluxes from the slab at intermediate subduction depths.

Results and preliminary interpretation

209 point analyses of F and Cl were made in serpentine (n=95), groundmass carbonate (n=104), calcite veins (n=10) and Cl-rich veins (n=6). These revealed pronounced variation in average F/Cl and halogen content of serpentine across the reaction zone from F/Cl=0.15 in the least altered serpentinite to 0.88 **in highly altered “ophicarbonate” adjacent to the listvenite front**. Groundmass carbonate showed complementary variation to co-existing serpentine, with mean F/Cl in each sample varying from 0.15 to 0.45. Listvenites showed even higher F/Cl ratios, averaging 41 and 50 in the two samples studied. There appears to be a marked difference in the listvenites between early forming magnesite to ferro-

magnesite vein networks and grains of dolomite and magnesite growing interstitially. The latter frequently show very high F/Cl ratios of up to 500 and suggest the potential involvement of a second fluid in the carbonation process. A similar bimodal distribution (though at lower F/Cl) is revealed by the halogen systematics in the serpentinites/ophicarbonates. Two distinct, correlated trends are apparent on a plot of F against Cl (Fig. 1). These divide the less altered samples earlier in the reaction zone from those closer to the listvenite front. These relationships may too suggest a plurality of fluids involved in the carbonation reaction or, alternatively, reflect a geochemical response to mineralogical changes in the serpentine (e.g. the crystallisation of talc as the reaction progresses). Overall, the progression towards higher F/Cl ratios in the carbonating serpentinites and fully-carbonated listvenites tends towards the composition of high F/Cl lithologies from the underlying metamorphic sole consistent with carbonation by fluid derived from subducting sediments and meta-basalts. Interpretation is ongoing to deconvolute the effects of mineral fractionation and fluid-chemistry. Analyses of Br and I in 2020 will aid greatly in developing our understanding of the origin of carbonating fluids and the evolution of their chemistry.

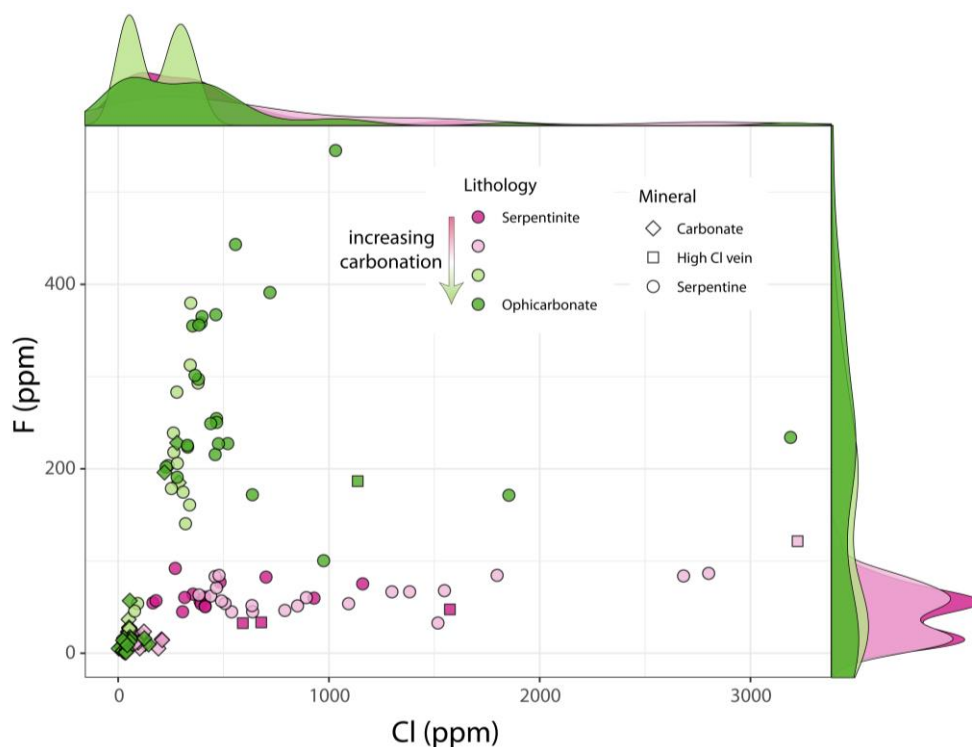


Figure 1. F versus Cl concentration (both in ppm) determined in serpentine and carbonates from across the reaction. Each colour represents a different sample progressing from least altered (pink) to most altered (green) immediately prior to the listvenite front. Two diverging trends are clear in the serpentines while co-existing carbonates show complementary trends at lower F and Cl.

References

- [1] Kelemen et al. (2011) *Annual Reviews of Earth and Planetary Science* 39, 545–576
- [2] Hilton, Fischer and Marty, 2002. *Reviews in Mineralogy and Geochemistry* 47, 319–370
- [3] Dilek & Furnes (2014) *Elements* 10(2), 93–100
- [4] Falk & Kelemen (2015) *Geochimica et Cosmochimica Acta* 160, 70–90

Water saturation and temperature changes affect halogen degassing of shallow magmas

M. Cassidy

Department of Earth Sciences, University of Oxford, Oxford, OX1 3AN UK

Motivation

I am attempting to understand how some halogens (Cl, F, Br) behave during temperature and water fluctuations within the shallow magma body, by measuring these elements in experimental glasses. The hypothesis being that these species partition between the melt and fluid phase as a function of temperature and water saturation, thus providing a means of detecting these changes in magma conditions by measuring volcanic gases at the surface.

Volcanic gas monitoring of active volcanoes mostly measures SO_2 and CO_2 , because previous experimental work has shown that the content of H_2O , CO_2 and SO_2 in the melt is predominantly controlled by pressure, therefore SO_2 and CO_2 are often used as proxies for deep magma ascent due to their different solubility depths [1,2]. However, many volcanic eruptions are directly sourced from magmas that reside from shallow reservoirs and not supplied by deeper mafic inputs to the system prior to eruption (e.g. Kelud volcano [3]). These eruptions are thought to be triggered instead by overpressures in the magma chamber due to cooling, crystallisation and volatile saturation [4]. In these instances, gas monitoring of traditional volatile species may be unable to detect changes relating to magma temperature and water saturation.

Recent studies suggest that the temperature of a residing magma reservoir may affect the explosivity of an impending eruption [3, 4, 5]. This is because temperature has a fundamental role in controlling **the magma's rheology, which determines the magma's ability to retain magmatic volatiles**. However, there is a poor understanding of how these gases and the halogens, partition from the melt and fluid phases at varying temperatures and water saturation conditions, in particular studies on Br partitioning are very rare. Some studies on Cl, suggest that its partitioning has a limited pressure dependence [6], offering promise for Cl and the other halogens, that temperature may be a key factor controlling its fluid/melt partitioning.

In my current work I have conducted petrological experiments at various pressures, temperatures and XH_2O (degree of water saturation in the fluid phase) on Kelud volcanics (Indonesia). I have constrained the magmatic storage conditions before both explosive and effusive eruptions. This work has unveiled shallow a magma storage body at 50-100 MPa, but with variable temperatures and XH_2O ratios between explosive & effusive eruptions [4]. The report focuses on measurements of Br, Cl and F contents of seven experimental glass products from Kelud and six experiments from Quizapu volcano, (Chile) and their natural starting materials. The samples chosen were ranged in compositions, basaltic andesite to dacite, pressures (50-120 MPa), temperatures 800°C – 1100°C and degrees of water saturation XH_2O (0.55 – 1). An average of ~7 analyses per sample were conducted, averages were calculated along with standard deviation (see figure below). The precision was good for water-saturated experiments, but there was more heterogeneity in the water under saturated experiments. Along with my unknown samples, secondary standards (GSE, BB1, BB2, BCR, T1G, ML3BG, and STHS6180), were also measured to check for reproducibility and accuracy. We found that the halogen concentrations for the secondary standards varied slightly between different mounts, supporting the notion that calibration should be conducted on the same mounts as the sample analysis if possible.

Outcomes

The data yield some interesting results (Fig. 1). In the basaltic andesite experiments, increased temperatures reduced the halogen concentrations measured in the glass (aka melt phase). The same overall trend also occurs for the water saturated dacite experiments.

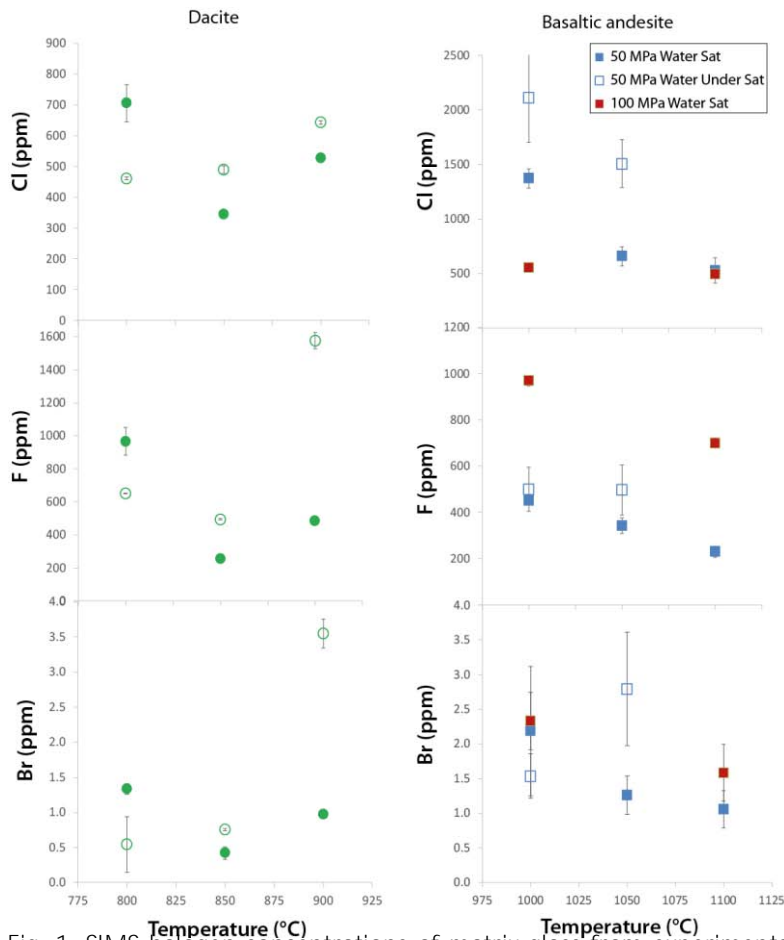


Fig. 1. SIMS halogen concentrations of matrix glass from experiments conducted at differing temperatures, pressures and degrees of water saturation. Open symbols refer to water undersaturated conditions.

partition to the fluid (or mineral) phase. In the volcanic system, H_2O , and CO_2 are less susceptible to changes in magmatic temperature, therefore if Cl, F and Br are not scrubbed by hydrothermal systems as they ascend to the surface, their relative ratios (e.g. decrease in HCl/CO_2) could provide key information to discern whether a magma is cooling, crystallising, or becoming water saturated leading up to an eruption.

Future work

The next steps with these data are to combine them with pre-existing Cl, F and Br data from experiments run at different temperatures, compositions, pressures and water saturation conditions. By collating these data and simulating their behaviour with volatile solubility models, I aim to more fully understand the water saturation and temperature dependence on halogen partitioning from the melt to the fluid and mineral phases, and its relevance for volcano gas monitoring.

References

- [1] Surono et al. (2012) *J. Volcanol. Geotherm. Res.* 241–242, 121–135. [2] Moor, J. M. et al. (2016) *J. Geophys. Res. Solid Earth* 1–15. [3] Cassidy, M. et al. (2016) *Geology* 44. [4] Cassidy, M., et al., (2019) *G Cubed*. 20, 8 4218-4247 [5] Ruprecht, P. & Bachmann, O. (2010). *Geology* 38, 919–922.

The depletion of halogens at $850^\circ C$ may be caused by enhanced apatite crystallisation, which could incorporate these halogens. Interestingly, the water undersaturated dacitic experiments display the opposite temperature trend as the water saturated experiments, for reasons yet unknown. There seems to be some pressure dependence on the partitioning (fluid/melt) of F, but less so for Br and Cl.

The results thus far show that the halogens do indeed partition from the melt to the fluid phase during temperature and water saturation changes within the magmatic body at shallow depths (especially Cl and Br, with partition co-efficients ($K_D^{Fluid/Melt}$) values >1 , see Fig. 2 below). The figure below for partition co-efficients for fluid/melt increasing with larger ionic radius is consistent with the literature. This trend is composition-dependent, halogens within more evolved dacitic melts will more strongly

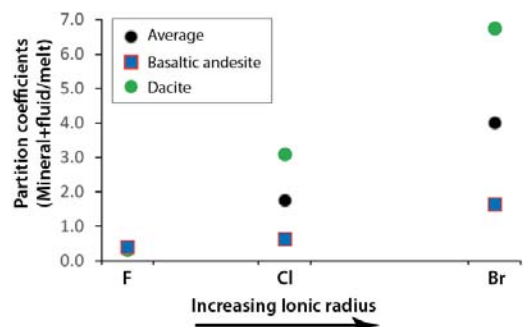


Fig. 2. $K_D^{Fluid/Melt}$ vs ionic radius for F, Cl and Br.

Oxygen isotope constraints on serpentinite dehydration in subduction zones

E.R. Clarke & J.C.M. de Hoog

School of GeoSciences, University of Edinburgh, Edinburgh EH9 3JW, UK

Introduction

Oxygen isotopes are commonly used in the measurement of equilibrium temperatures of mineral pairs. This project aimed to determine if serpentine and its dehydration product olivine in high-pressure Alpine serpentinites were in O isotopic equilibrium to further investigate the observation that considerable disequilibrium was present for B isotopes. As IMF did not have an antigorite O isotope standard of appropriate composition, the first step was to characterise such a standard. As the first author graduated before sample data could be collected, this project was unfortunately not completed.

No serpentine-olivine geothermometer exists in the literature, however, it can be calculated from serpentine-magnetite ($10^3 \ln \alpha_{\text{srp-mt}} = 1.81 \times 10^6 / (T(K))^2 + 1.41$) [1] and olivine-magnetite ($10^3 \ln \alpha_{\text{ol-mt}} = 2.62 \times 10^6 / T(K)^2$) [2] equilibria. Using these equations, the equilibrium between serpentine and olivine can be expressed as $10^3 \ln \alpha_{\text{srp-ol}} = 0.81 \times 10^6 / T(K)^2$ (Fig. 1).

Sample characterisation

When conducting SIMS measurements it is vital to have calibration standards of a similar composition to the samples. FeO especially can greatly affect the instrument mass fractionation (IMF) of O isotopes (Craven, personal comm.) We collected a ca. 10 cm long dark-green serpentine specimen from **46°01'01"N and 7°50'32"E** near Zermatt, Swiss Alps. The piece (ZS17-DS) was not in-situ. It was analysed semi-quantitatively by SEM-EDS at EMMAC and has 2.3 wt% Al₂O₃ and 5 wt% FeO.

Whole rock O isotopes were analysed at SUERC by Adrian Boyce. Four aliquots of ZS17-DS were taken and each aliquot was split in four. Two aliquots were run with <1hr pre-fluorination, the other two were preceded by a degassing stage at 200°C in vacuo, and then <1hr pre-fluorination. The two methods differed by 0.19‰, which is within error, but the preheated samples gave more consistent results and are the ones reported here, averaging to $\delta^{18}\text{O}_{\text{VSMOW}} = 6.26 \pm 0.15$ (1s, n=7).

Four different aliquots were mounted in different orientations in an epoxy mount to check for homogeneity by SIMS. Three aliquots polished well and produced consistent results in agreement with whole-rock data. Serp-D did not polish well, possibly due to the orientation, and produced slightly anomalous results. This could point to an orientation effect but more likely it was due to the poor polish of the sample.

Table 1. Results of O isotope homogeneity test of serpentine ZS17-DS by SIMS

	Serp-A	Serp-C	Serp-D	Serp-E
Average (n=30)	6.4‰	6.8	7.8‰	6.3‰
St.Dev. ‰ (1s)	0.52	0.34	0.36	0.38

References

Agrinier and Cannat, 1997 Chiba et al., 1989

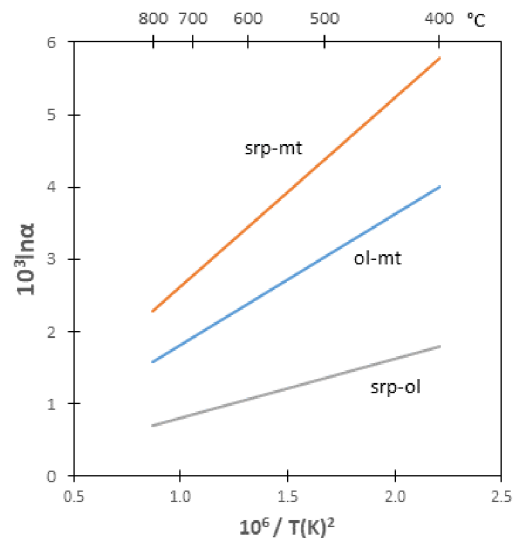


Fig. 1. Oxygen isotope fractionation between serpentine, olivine and magnetite vs. T, where $\alpha = [^{18}\text{O}/^{16}\text{O}_{\text{min1}}] / [^{18}\text{O}/^{16}\text{O}_{\text{min2}}]$.

Boron isotope partitioning between fluid and olivine

E.R. Clarke¹, J.C.M De Hoog¹ & G. Bromiley¹

¹School of GeoSciences, University of Edinburgh, Edinburgh EH9 3JW, UK

Introduction

Boron isotopes in subduction zones have proven to be a useful geochemical tool to track the origin of fluids contributing to arc magmas, and show an important role for serpentinite dehydration [1,2]. However, there is a lack of data on the equilibrium fractionation of the isotopes in ultramafic rocks, in particular a lack of fluid-mineral B isotope fractionation data for serpentinites^[2]. Not knowing how B partitions between ultramafic minerals and fluid limits our ability to understand the deep B cycle. Therefore, we performed olivine-fluid experiments to constrain B isotope partitioning between these two phases and the influence of fluid pH. With these data we can will be more able to accurately predict the B and $\delta^{11}\text{B}$ composition of serpentinite dehydration fluids and the contribution of these fluids to the B cycle.

Methods and experimental results

Olivine was grown in the presence of a B-rich aqueous fluid at different temperatures and pH conditions to determine $\Delta^{11}\text{B}_{\text{ol-fl}}$ and its dependence on these different conditions. A single platinum capsule (4mm diameter) was filled with fluid and starting mix (comprising powdered SiO_2 , MgO and $\text{B}(\text{OH})_3$) and welded at both ends. The fluid was added with a B-free microlitre pipette to the bottom of the capsule, to avoid evaporation on welding. The type of fluid changed depending on the required pH, for the acidic experiments just distilled water was added and for the alkaline experiments a 0.3M NaOH solution.

Table 1. Boron concentration and $\delta^{11}\text{B}$ data for olivine-fluid experiments.

Temp (°C)	pH	$^{F/O}D_B$	$\Delta^{11}\text{B}_{\text{ol-fl}}$		B ppm	B error	$\delta^{11}\text{B}$	$\delta^{11}\text{B}$ error
1000	acid	23.9 ± 2.5	-2.7 ‰ ± 1.7 ‰	Olivine	223	± 22.9	-2.3 ‰	± 1.7 ‰
				Fluid start	6158	0	+0.0 ‰	0*
				Fluid end	5338	± 81.2	+0.4 ‰	± 0.3 ‰
1100	acid	26.1 ± 2.9	-2.4 ‰ ± 2.0 ‰	Olivine	206.3	± 22.8	-2.1 ‰	± 2.0 ‰
				Fluid start	6161.2	0	+0.0 ‰	0*
				Fluid end	5375.2	± 87.6	+0.3 ‰	± 0.3 ‰
900	acid	52.4 ± 3.7	-3.6 ‰ ± 0.6 ‰	Olivine	97.3	± 6.8	-3.4 ‰	± 0.6 ‰
				Fluid start	5426	0	+0.0 ‰	0*
				Fluid end	5101.2	± 22.2	+0.2 ‰	± 0.04 ‰
1000	alk	12.9 ± 0.5	-4.9 ‰ ± 1.0 ‰	Olivine	373.1	± 12.6	-3.8 ‰	± 1.0 ‰
				Fluid start	6203.1	0	+0.0 ‰	0*
				Fluid end	4808.6	± 47.6	+1.1 ‰	± 0.3 ‰
1100	alk	91.2 ± 14.7	-4.5 ‰ ± 1.0 ‰	Olivine	69.7	± 11.3	-4.3 ‰	± 1.0 ‰
				Fluid start	6636.7	0	+0.0 ‰	0*
				Fluid end	6358.9	± 44.1	+0.2 ‰	± 0.05 ‰

* Fluid starting values were calculated using weight of fluid and $\text{B}(\text{OH})_3$ added to capsule. Fluid end values are mass balanced.

Each experiment was run between 1.95 to 2.5 hours at 1600 °C first to homogenise the mixture and then lowered to the run temperature and left between 46.6 to 48.3 hours. We did not make porosity estimations, but it was clear that each experiment was porous from the inflated shape of the capsule

after the experiment, loose grains and micron-scale holes. This indicates that fluid was present and able to equilibrate with the olivines during the experiment. Fluid/rock ratios varied between 0.25 and 0.3. Some minor pyroxene (<1%) was present in the run products, but in too small quantities to influence the results.

Results and discussion

Table 1 shows the results of our experiments, which are summarised in Fig. 1. The acidic fractionation has a similar gradient ($1000/T(K)$ vs $\Delta^{11}B_{ol-fl}$) to other published experiments not including olivine (-9.45 vs -10.12 respectively)[3]. However, the fractionation line in Fig.1 is roughly **2-3 ‰ higher**. This suggests that olivine has a greater preference for ^{11}B than other silicates (or at least the ones involved in previous $\Delta^{11}B_{mineral-fluid}$ calculations). But olivine also shows a preference for ^{10}B compared to acidic fluid. One possible explanation is that olivine incorporates B in both tetrahedral and trigonal coordination. At 2 GPa, the breakdown of antigorite occurs between 500 and 700°C. According to the extrapolation on Fig. 1 the $\Delta^{11}B_{ol-fl}$ at these temperatures will be -7.5 to -5 ‰ in acidic conditions. Based on this data, the B concentration of the fluids eventually driven off dehydrating serpentinites could be 4-22% lower than the B concentration of the fluids initially produced by serpentine breakdown, just by the retention of B in secondary olivine and pyroxene.

Conclusions

This data suggests that B coordination in olivine is different to other silicates and fluid. This can be explained by B being both trigonally and tetrahedrally coordinated in olivine. This preference changes with pH: in a more acidic pH there is a higher preference for ^{11}B (trigonal) and in a more alkaline pH there is a higher preference for ^{10}B (tetrahedral). This work may also have some broader implications for the B cycle. B mixing diagrams predict that a fluid with 60 to 80% (acidic fluid pH) deserpentinization fluid is needed to mix with the mantle to explain the B composition the majority of arc lava magmas. This suggests that serpentinites dominate the B budget of the down going slab. However, before these claims can be substantiated further experiments should be run for consistency and to expand the tested window of pH and temperature.

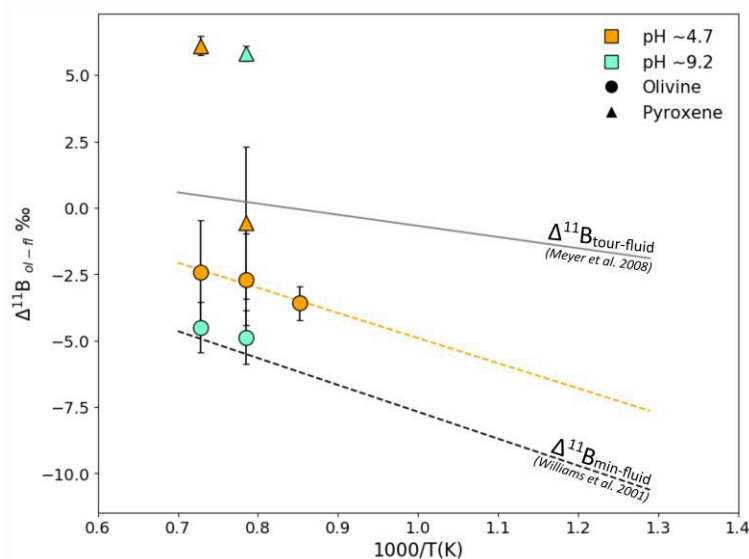


Fig. 1. $\delta^{11}B_{ol-fl}$ vs $1000/$ Temperature (Kelvin) for all five successful experiments. There is a positive correlation between $\Delta^{11}B_{ol-fl}$ and temperature which for the acidic experiments has been extended to lower temperatures (orange dashed line). This extrapolation is compared to other published $\delta^{11}B$ studies: $\Delta^{11}B_{min-fl}$ where mineral= illite Williams et al. (2001) and $\Delta^{11}B_{tour-fl}$ from Meyer et al. (2008). Illite incorporates tetrahedral B and tourmaline incorporates trigonal B.

References:

- [1] De Hoog JCM & Savov IP (2018) Boron isotopes as a tracer of subduction zone processes, *in* Boron Isotopes. Advances in Isotope Geochemistry, Springer, p. 217–247.
- [2] Marschall HR (2018) Boron isotopes in the ocean floor realm and the mantle: *in* Boron Isotopes. Advances in Isotope Geochemistry, Springer, p. 189–215.
- [3] Williams LB, Hervig RL, Holloway JR & Hutcheon I (2001) *Geochim. Cosmochim. Acta* 65, 1769–1782.

Volatile degassing styles and the triggering of an eruptive event in an open, persistently degassing volcanic system, Villarrica volcano, Chile

J.A. Cortés¹ & E.S. Calder²

¹ Department of Geography and Geology, Edge Hill University, St Helens Road, Ormskirk, L39 4QP, UK

²School of GeoSciences, University of Edinburgh, Edinburgh EH9 3JW, UK

Summary

H₂O and CO₂ content were measured in olivine-hosted melt inclusions (MI), collected from the products of major eruptions (1971, 1984 and 2015) and the background activity (1999 – 2012) from Villarrica volcano, Chile, to track for any relationships between volatile content and eruptive style. While we have found roughly that the products from a relatively more violent eruption are comparatively richer in volatile content than products erupted during the background activity, there are important differences between different types of eruptions. Compositions of the MIs and host-olivine crystals also show substantial differences depending on the eruptive event.

Results

We separated olivine crystals from the 1971, 1984, 2015 major eruptions and from background activity between 1999 and 2000. Individual olivine crystals were mounted in epoxy resin and both olivine and hosted MI were first analysed using the electron microprobe. Compositionally, the olivine crystals from the 2015 eruption show a substantial more spread in compositions between Fo₇₂ and

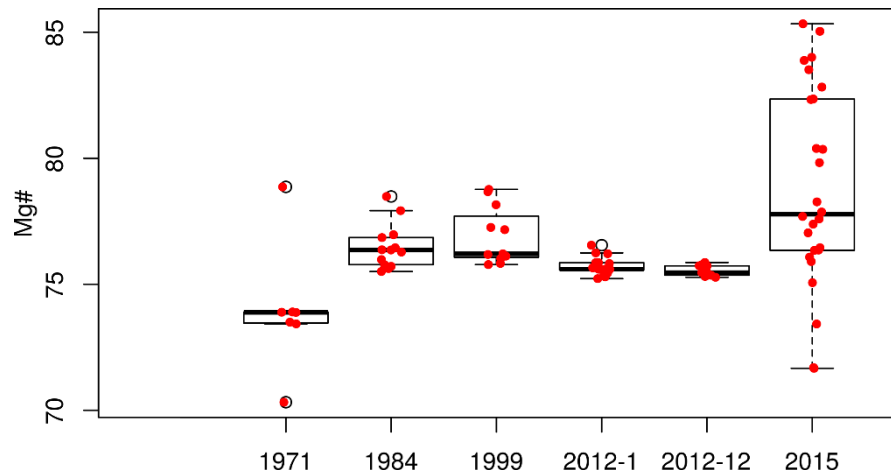


Figure 1. Box-Plot with the range in olivine compositions as Mg number from major eruptions (1971, 1984, 2015) and background activity (1999, 2000-1, 2000-12).

Fo₈₅ than other eruptive events or the background activity (Fig. 1). Collected olivine crystal from the 1971 eruption cluster tightly around Fo₇₃, ranging from Fo₇₀ to Fo₇₉, while olivine crystals from the 1984 eruption are indistinguishable from background activity olivine mineral chemistry.

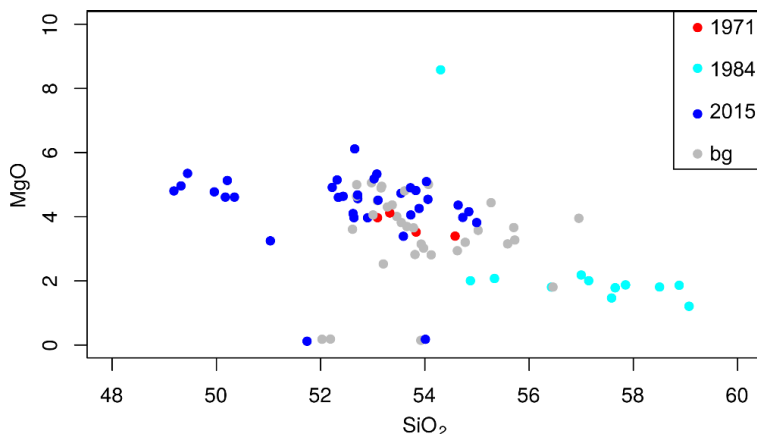


Figure 2. MgO vs. SiO₂ variation diagram of MI hosted in olivine inclusions from 1971 eruption (red solid circles), 1984 eruption (cyan solid circles), 2015 eruption (blue solid circles) and background activity (grey circles).

MI compositions also show remarkable differences between eruptions and the background activity, and between the different eruptions. MI hosted in olivine from the 2015 eruption have primitive to intermediate compositions, the latter similar to MI from 1971 and the background activity. MI from the 1984 eruption seems to be more evolved than any other MI analysed during this study (Fig. 2).

Volatile content measured in the MI inclusions show a solubility pattern mostly consistent with open system degassing using [1] solubility model (Fig. 3). Samples from 1971 eruption seem to be mainly degassed of CO₂ while background samples are mostly degassed in both H₂O and CO₂. Samples from the 2015 eruption are comparatively richer in these volatiles, although the most enriched sample contain ~500 ppm of CO₂ and ~1.5 wt% of H₂O. Few analyses from samples of the 2015 and 1984 eruptions seem to be H₂O-degassed but they contain between 100 up to 250 ppm of CO₂, not consistent with the theoretical solubility model such as [1]. This behaviour can be explained with a process of non-equilibrium degassing in the system, which, according with experimental data [2], seems to preserve higher CO₂ content than H₂O in solution, simply because, although CO₂ is more insoluble than H₂O, the kinetic of exsolution is less efficient in a sudden decompression event.

Preliminary Conclusions

Results strongly suggest that the 2015 eruption was triggered by the sudden arrival of basaltic recharge (Figure 2) that decompress under non-equilibrium conditions, thus preserving a comparatively CO₂-richer than a theoretical solubility model. Based on the MI with the highest volatile content (Figure 3), these MI were trapped at a pressure of between 600 to 1000 bars, suggesting a depth of no more than 3 Km for the ascending melt. Some MI measured in products of the 1984 eruption seem to suggest an analogue non-equilibrium mechanism but shallower depths of entrapment. Products from the 1971 eruption show evidence of open system degassing, which is also observed in the mostly degassed background activity samples with the occasional samples in disequilibria.

References

- [1] Papale, P., Moretti, R. & Barbato, D. (2006). The compositional dependence of the saturation surface of H₂O + CO₂ fluids in silicate melts. *Chemical Geology* 229, 78–95.
- [2] Pichavant, M., Di Carlo, I., Rotolo, S.G., Scaillet, B., Burgisser, A., Le Gall, N., Martel, C., (2013) Generation of CO₂-rich melts during basalt magma ascent and degassing. *Contributions to Mineralogy and Petrology* 166, 545-561.

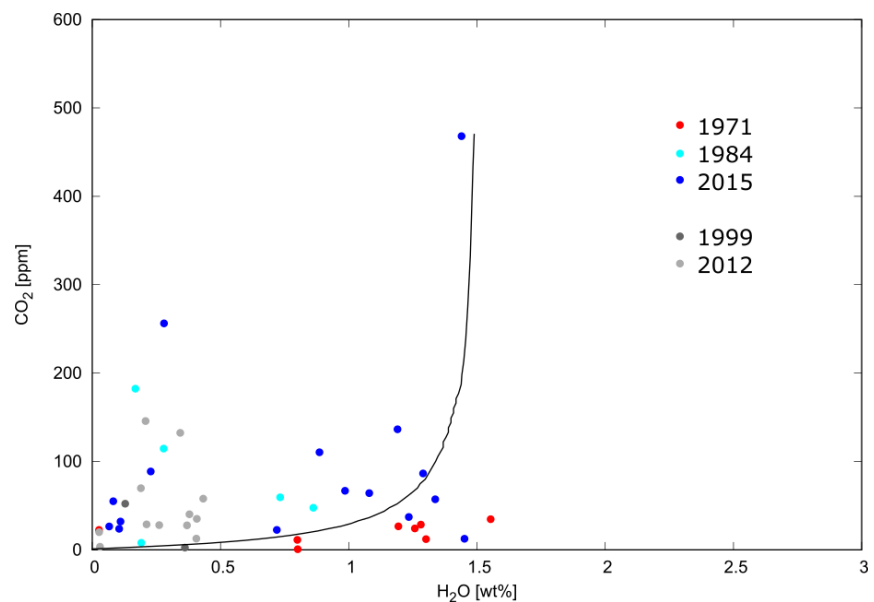


Figure 3: CO₂ and H₂O volatile content measured in MI hosted in olivine inclusions from 1971, 1982, 2015 eruptions and background activity. Symbols as in Figure 2.

The source and flux of volatiles in off-craton lithospheric mantle

James C. Crosby¹, Sally A. Gibson¹, Teal R. Riley², Fin M. Stuart³

¹Department of Earth Sciences, University of Cambridge, Cambridge, CB2 3EQ, UK

²British Antarctic Survey, Natural Environmental Research Council, Cambridge, CB3 0ET, UK

³Isotope Geosciences Unit, Scottish Universities Environmental Research Centre, Glasgow, G75 0QF, UK

Motivation for SIMS project

Models of global volatile cycles predict that **Earth's mantle represents** a major storage reservoir for CO₂, H₂O, S, F, Cl together with B. Nevertheless, the abundances of these volatiles are poorly constrained in phases that constitute the bulk of the mantle. The non-convective, upper-most, solid mantle that underlies **Earth's** crust is known as the lithospheric mantle and potentially represents a major reservoir for volatile elements [1]. This is especially true in continental settings where CO₂, H₂O, B, S, F and Cl may have been accumulating for billions of years. These volatile elements are incorporated into mantle phases during infiltration of metasomatic agents including: (i) melts and fluids from subducting slabs; and (ii) small-fraction, volatile-rich melts sourced from the depleted or primitive mantle (Fig. 1). Metasomatised lithospheric mantle may accommodate substantial concentrations of volatiles in: (i) accessory minerals, such as phlogopite, amphibole and apatite (0.55 wt.% Cl and 3.4 wt.% F); or (ii) the much more abundant nominally volatile-free phases (e.g. olivine and pyroxene [2]). While subduction-related metasomatism leads to H₂O, B and Cl/F enrichment [3,4], low-degree silicate melts from the convecting mantle cause CO₂ and F/Cl enrichment [5]. Our project is primarily focussed on off-craton lithospheric mantle because volatiles in this reservoir are susceptible to mobilisation as a consequence of small perturbations of the geotherm and may have dramatic environmental consequences that **impact on Earth's biosphere** [6]. The greatest release of CO₂, B, H₂O, S, F and Cl from the lithospheric mantle is expected to occur during the impact of high temperature mantle plumes that are associated with the formation of Large Igneous Provinces (e.g. Deccan & Siberian Traps).

Samples analysed by SIMS

For this project, we selected global suites of off-craton mantle xenoliths of varying petrology, tectonic setting, and metasomatic history (Fig. 1, Table 1). These xenoliths provide an excellent basis to quantify how different types of metasomatism affect the volatile budget of the lithospheric mantle. Furthermore, by combining this data with the results of a helium isotope study (³He & ⁴He) we will potentially be able to constrain volatile input from different reservoirs of Earth.

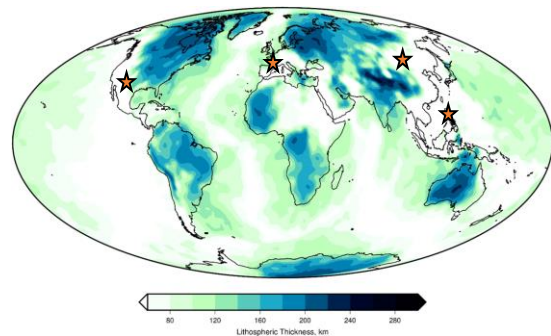


Figure 1. Locations of samples relative to a map of global lithospheric thickness [7]

Table 1 summarising the location, metasomatic history, petrology and tectonic setting of all samples analysed

Sample	Location	Metasomatised (La/Yb > 1)	Peridotite or pyroxenite	Intra-continental or subduction zone?
KH1	Kilbourne Hole	No	Clinopyroxenite	Intra-continental rift
KH4	Kilbourne Hole	No	Peridotite	Intra-continental rift
DW3	West Eifel	Yes	Peridotite	Intra-continental rift
DW5	West Eifel	Yes	Clinopyroxenite	Intra-continental rift
G17	West Eifel	Yes	Peridotite	Intra-continental rift
TM2	Tariat	No	Peridotite	Intra-continental rift
J1A	Ichinomegata	Yes	Peridotite	Subduction zone

SIMS analysis of off-craton xenoliths and analytical standards

The samples were analysed using the new Cameca 7f-Geo. For olivine and orthopyroxene, H and F were calibrated using OPX-KH03-4 and OPX116610. For clinopyroxene, H and F were calibrated using CPXKH03-4, CPX-SC-J1, and CPX-SMC331139. All chlorine concentrations were calculated using St8.1.A9.

Table 2. Standards used during SIMS analysis, those marked with a '*' were used for calibration.

Standard	Olivine analysis	Orthopyroxene analysis	Clinopyroxene analysis
AVL516-4-1	Y*	Y*	Y
OL116610	Y	Y	Y
OLDC0121	Y	Y	
OL-Fo	Y*	Y*	
OPX-KH03-4	Y	Y	
OPX1166	Y	Y	
ST8.1.A9	Y*	Y*	Y*
CPX-KH03-4			Y*
CPX-SC-J1			Y*
CPX-SMC e31139			Y*

Results

Overall, when compared with major and trace element mineral chemistry, this data agrees with the most recently published information from Gibson et al. [8], whereby, pyroxenites have a very high volatile content of H, F, and Cl relative to peridotites. The new SIMS volatile data will build on this previous work by: (i) quantifying sub-solidus re-equilibration between orthopyroxene and clinopyroxene and (ii) substitution mechanisms in shallower (spinel-facies) mantle. Novel comparisons with an ongoing investigation on helium isotopes in the same samples will provide exciting insights to the origins of volatile enrichment in the lithospheric mantle.

Table 3. Ranges of H, F and Cl in olivine, orthopyroxene and clinopyroxene.

Standard	Olivine analysis (ppm)	Orthopyroxene (ppm)	Clinopyroxene (ppm)
H	0 – 2.1	77.2 – 231.2	206 – 484
F	2.3 – 4.9	4.5 – 15.7	2.8 – 64.9
Cl	3.7 – 5.9	4.1 – 13.2	3.4 – 8.2

Importance of SIMS results

The SIMS results for the four xenolith locations contribute to the first ever internally-consistent dataset that includes volatile elements (H, CO₂, Cl, F,) major elements (e.g. SiO₂), trace elements (e.g. U, Th, La, Yb), and noble gas isotopes (³He/⁴He). The results are promising and allow us to place improved constraints on the nature and origin of metasomatic enrichment of the lithospheric mantle beneath three **of the world's major** continental rift zones. These are locations where the lithospheric mantle reservoir is believed to significantly contribute to the volatile contents of melts erupted by rift-related volcanoes.

References

- [1] Liu et al. (2011) *Geology* 39, 923-926; [2] Bernard et al. (2017) *Geochim. Cosmochim. Acta* 199, 324-350; [3] Li et al. (2008) *J. Geophys. Res.* B 113, 1-22; [4] Barnes et al. (2018) 805-845; [5] Ferzzotti & Ferrando (2018) 805-845; [6] Song et al. (2011) *Geology* 39, 739-742; [7] Priestley & McKenzie (2008) *Lithos* 102, 1-11; [8] Gibson et al. (2020) *Geochim. Cosmochim. Acta*. <https://doi.org/10.1016/j.gca.2020.02.018>

Investigating the fossilisation and nature of sulphur metabolisms within associated fossil vent animals and microbes

M.N. Georgieva¹, C.T.S Little², R.J. Herrington³ & A.G. Glover¹

¹Life Sciences Department, Natural History Museum, London SW7 5BD, UK

²School of Earth and Environment, University of Leeds, Leeds LS2 9JT, UK

³Earth Sciences Department, Natural History Museum, London SW7 5BD, UK

Background

Hydrothermal vents in the modern deep sea are inhabited by remarkable communities of highly specialised animals, which are dependent on chemosynthesis carried out by prokaryotes. Microbes capable of sulphide oxidation are particularly important for primary production at vent sites, and many vent animals have intimate and diverse associations with bacteria that enable them to thrive within vent environments [1]. For example, the tube-dwelling vent annelid worm *Ridgeia piscesae* obtains all of its nutrition from sulphide oxidising endosymbionts [2], while another vent annelid tubeworm, *Alvinella pompejana*, grazes on mats of filamentous bacteria that attach to its outer body wall and inner tube surface [3]. The microbial communities living on and around vent animals exhibit diverse metabolic pathways that include both sulphur oxidation and sulphate reduction [4–6], and the development of symbioses between animals and microbes is regarded as a key adaptation in enabling animals to successfully colonise vents, thus evolving to become the specialised vent fauna that occupies vents today [1,7]. Understanding the nature of these associations in geological time is crucial to unravelling the history of animal colonisation of vents.

The importance of hydrothermal vents as habitats for animals throughout Earth history is evidenced by the fossil record of these environments [8], with the oldest vent community that includes animals occurring within the Silurian Yaman Kasy volcanic-hosted massive sulphide deposit, Urals, Russia [9]. While it may be supposed that ancient vent animals would have also relied on microbes for their nutrition, nothing is known about the ways in which they interacted with them. Using new findings that reveal the detailed fossilisation of microbes associated with both recently-mineralised and ancient fossilised animals from hydrothermal vents [10], as well as newly acquired pathfinder $\delta^{34}\text{S}$ data, this project aimed to use sulphur isotopes to explore the fine-scale preservation and nature of metabolic pathways of fossilised vent animals and associated microbes. Specifically, sulphur isotopic data was used to examine whether pyrite preserving hydrothermal vent animals and microbes has a distinct sulphur isotopic signature to non-fossiliferous pyrite from the host deposit, and determine whether isotopic signatures are indicative of particular sulphur cycling pathways for fossil vent fauna. Unravelling the metabolisms of ancient vent animals and microbes through sulphur isotopes will synthesise understanding of the nature of animal-microbial associations, crucial to the adaptation and diversification of animals into vent environments, throughout evolutionary time.

Results

We were initially assigned a one-day session on the IMF Cameca 1270 SIMS instrument in February 2019, during which a total of 63 sulphur isotopic analyses of pyrite, and 48 measurements of BalMat pyrite standard were performed on two samples. These samples represented recently-mineralised tube walls of the hydrothermal vent annelids *Alvinella* sp. and *Ridgeia piscesae*. During July-August 2019, an additional 236 sample and 151 standard measurements were acquired, of material representing ancient vent fossils dating to the Early Jurassic and Early Silurian.

Pyrite delineating fossilised vent animals exhibiting three different types of textures was targeted for the above analyses, based on the main texture types observed with the specimens: pyrite containing microbial fossils, pyrite with a rough texture with no microbial fossils, and pyrite with a smooth texture not containing microbial fossils. Subsequent SEM imaging of SIMS pits revealed that the measurement spot size achieved was approximately 5 μm .

The above measurements showed distinct differences in $\delta^{34}\text{S}$ between pyrite of the three different

texture types (Figure 1). Pyrite containing microbial fossils exhibited consistently lighter $\delta^{34}\text{S}$ values compared to both smooth and porous pyrite present within the same sample, with t-tests demonstrating these differences to be significant ($p < 0.001$). For vent fossils which do not contain microbial fossils, the data we have acquired so far also demonstrates consistent differences between pyrite of a smooth texture and roughly-textured pyrite, with roughly-textured pyrite exhibiting significantly lighter $\delta^{34}\text{S}$ values in all but one sample (P23946-YKS).

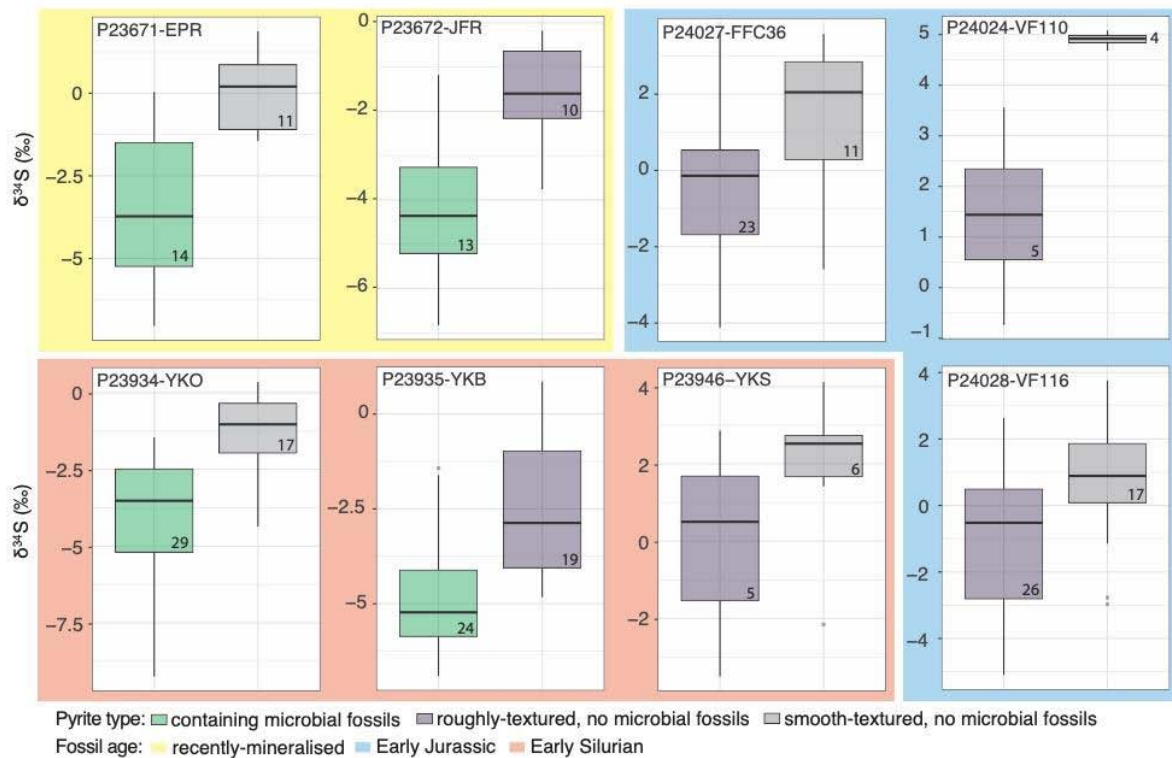


Figure 1. Boxplots paired by hydrothermal vent fossil sample, demonstrating results of $\delta^{34}\text{S}$ measurements in pyrite of different textures present within those samples (indicated by boxplot colour). Numbers in bottom-right corner of boxplots indicates number of measurements, while 'P' labels indicate sample name. Boxplots are grouped according to the fossil age (indicated by background colour).

Discussion

The observed differences in $\delta^{34}\text{S}$ between pyrite of varying texture in the hydrothermal vent fossils analysed firstly indicates that microbes very likely do affect the pyrite that fossilises them, leaving a potential metabolic fingerprint. This can be observed in both recently-mineralised hydrothermal vent fossils as well as in ancient material approximately 440 Ma in age. The inferred metabolic pathway that is most likely for these microbes based on the observed $\delta^{34}\text{S}$ values is sulphide oxidation, which has been demonstrated to produce clear but small to moderate (1-10‰) fractionations in $\delta^{34}\text{S}$. The smaller differences in $\delta^{34}\text{S}$ between the rough- and smoothly-textured pyrite are possibly due to interaction with organic matter during pyrite formation, but warrant further investigation.

References

- [1] Dubilier, N. *et al.* (2008) *Nat. Rev. Microbiol.* 6, 725–740; [2] Feldman, R.A. *et al.* (1997) *Mol. Mar. Biol. Biotechnol.* 6, 268–277; [3] Gaudron, S.M. *et al.* (2012) *Mar. Environ. Res.* 77, 129–40; [4] Prieur, D. *et al.* (1990) *Mar. Biol.* 106, 361–367; [5] Cottrell, M.T. and Cary, S.C. (1999) *Appl. Environ. Microbiol.* 65, 1127–1132; [6] Lopez-Garcia, P. *et al.* (2002) *Environ. Microbiol.* 4, 204–215; [7] Sun, J. *et al.* (2017) *Nat. Ecol. Evol.* 1, 0121; [8] Little, C.T.S. *et al.* (1998) *Geol. Soc. London, Spec. Publ.* 148, 259–270; [9] Little, C.T.S. *et al.* (1997) *Nature* 385, 146–148; [10] Georgieva, M.N. *et al.* (2018) *Proc. R. Soc. B Biol. Sci.* 285, 20182004

Can drips or delamination generate the Eoarchaeon continental crust?

Alan R. Hastie

School of Geography, Earth and Environmental Sciences, University of Birmingham, B15 2TT

Scientific reasons for the investigation

The mechanism **responsible for forming Earth's first stable continental crust** in the Eoarchaeon-Palaeoarchaeon (4.0-3.6 Ga) is commonly attributed to magmatism in subduction zones. However, previous high pressure-temperature (P-T) experiments, that reproduce primitive subduction environments, only replicate a limited volume of early continental material. Therefore, new high P-T experiments, replicating another proposed crustal formation mechanism (drips and/or delamination), have recently been undertaken using novel starting material. Trace element analyses are now required on these melts to confirm if they have compositions similar to the oldest continental crust.

Background

Crustal drips (dripduction) and lower crustal delamination predominantly involve the base of the early Archaean mafic crust becoming ductile, foundering into the mantle, and undergoing partial melting on descent. Although the thickness of an Eoarchaeon-Palaeoarchaeon mafic crustal lid is uncertain (from 25-45 km), in order for the lower crust to sink it must become denser than the underlying mantle. The density of lower crustal granulites can be increased by stabilising garnet, which, although heavily dependent on composition, commonly begins to stabilise in anhydrous tholeiitic metabasic compositions at pressures approximating 1.4 GPa. Consequently, crustal drips and delaminations will probably undergo fusion at pressures higher than 1.4 GPa.

Project Hypothesis

Trace element compositions similar to Eoarchaeon-Palaeoarchaeon continental crust can be formed by partial melting of mafic source regions in lower crustal drips and delaminations >1.4 GPa.

Objective

Here, 8 new high P-T experiments at ~45-90 km (1.4-2.8 GPa) have been performed using primitive oceanic plateau starting compositions from the Ontong Java Plateau (OJP). All of our new experiments generated partial melt pools from 10-**100µm in diameter in equilibrium with** an eclogite facies mineral assemblage containing garnet and clinopyroxene. We now need to confirm that the trace element compositions of these new partial melts are similar to Eoarchaeon-Palaeoarchaeon continental crust compositions. Our overall objective is: analyse melt pools from new high P-T experiments to determine if the unique trace element composition of the Eoarchaeon-Palaeoarchaeon continental crust can be generated by partial melting of Eoarchaeon-Palaeoarchaeon lower crustal drips and delamination using Mesozoic oceanic plateau as crustal analogues.

Preliminary results

Some results are still pending on a final visit to the facility in April 2020 (likely to be postponed by a number of months now due to the global Covid-19 situation). Preliminary analyses of the partial melts from the four experiments (OJPga7-9 and OJPgw33) are seen in Fig. 1. As can be seen, the new melts do have many elemental compositions that match the oldest continental compositions (ETT in Fig.1).

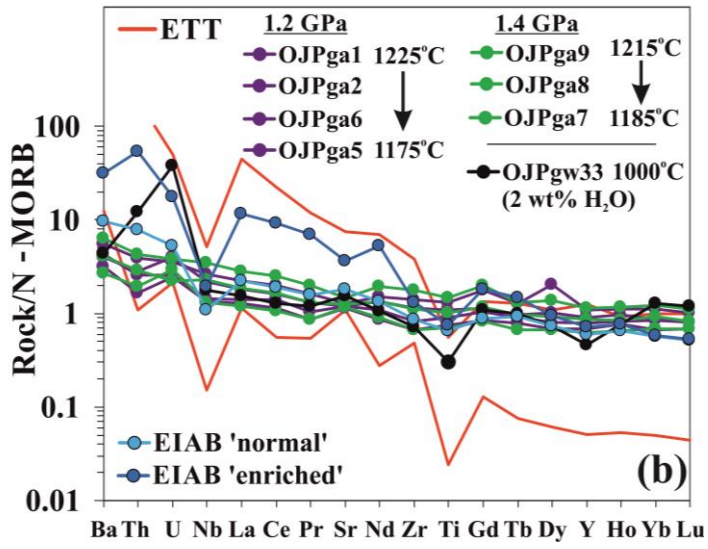


Figure 1. Preliminary analytical results.

Trace element partitioning between sulphate phases and silicate melts in arc magmas

M.C. Hutchinson, R.A. Brooker & J.D. Blundy

School of Earth Sciences, University of Bristol, Bristol, BS8 21RJ, UK

Introduction

Recent studies indicate that anhydrite may be a common, if rarely preserved, igneous phase in arc magmas, particularly in high-sulphur magmas related to the formation of magmatic-hydrothermal ore deposits [1]. Furthermore there is evidence (including the experiments analysed in this study), that immiscible sulphate melts may be stable in sulphur rich magmas at high temperature. To date, little data has been published relating to the partitioning of trace elements between sulphate phases and silicate melts. The aim of this study was to provide partition coefficients for a range of trace elements based on the analyses sulphate melt, silicate melt and anhydrite equilibrated at a range of P-T conditions.

Results

Upon quenching, sulphate melts form a mass of finely intergrown, heterogeneous, quench products, which makes the analysis of the bulk composition difficult. As such, partition coefficients calculated by SIMS analyses have been compared to both LA-ICP-MS analyses (Fig. 1), and mass balance calculations, and in general show excellent agreement.

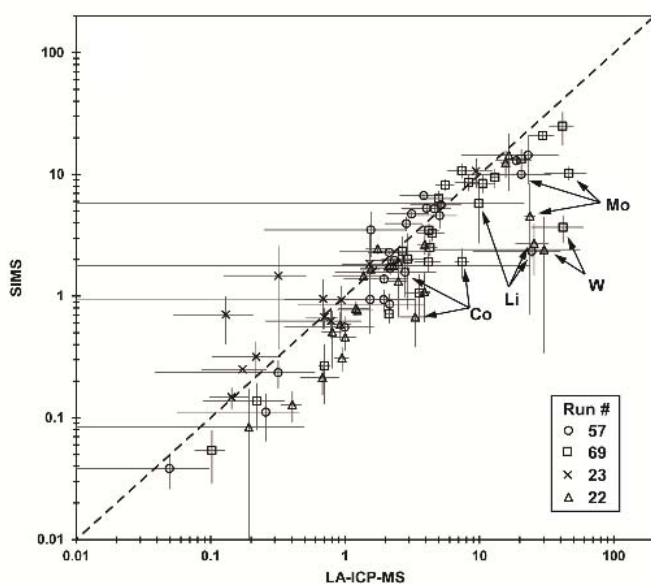


Figure 1. Comparison of sulphate melt - silicate melt partition coefficients calculated from SIMS and LA-ICP-MS analyses.

Sulfate melt – silicate melt partition coefficients, plotted as a function of their charge and effective ionic radius (Z/r , Fig. 2), appear to vary systematically, with peaks in compatibility in the sulphate melt close to the dominant cations, Ca^{2+} and S^{6+} . This is consistent with a melt which retains a relatively high degree of the structural ordering based around Ca^{2+} cations and anionic SO_4^{2-} groups. Pairs of elements with similar Z/r (e.g. Ho-Y, Zr-Hf, Nb-Ta) generally show similar partitioning behaviour, as expected.

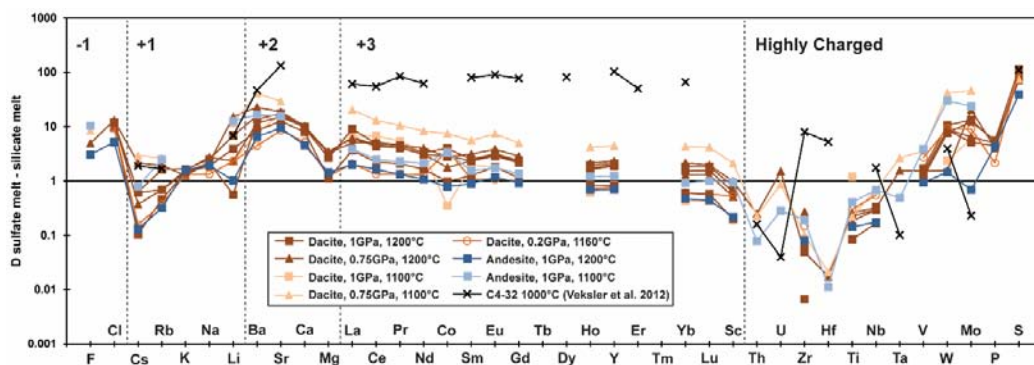


Figure 2. Sulfate melt - silicate melt partition coefficients arranged by Z/r . F, U, Th, Hf, Ta from SIMS, other elements based on LA-ICP-MS or EPMA analyses

Calculated D values from this study are in many cases significantly lower than previously published values [2], which is likely attributable to differences in the silicate melt composition between these two studies.

Anhydrite – silicate melt partition coefficients determined by SIMS analysis (Fig. 3) indicate that +2 and +3 cations, which are close in size to Ca^{2+} (i.e. Sr and light-middle REE), show a preference for anhydrite whereas smaller +2 cations (Sc, Mg, Mn) and +1 cations (Li, Na, K, Rb) strongly favor the silicate melt. The parabolas formed on plots of $\log D_i$ versus ionic radius (Onuma diagrams, Fig. 3), are well fit by lattice-strain models and illustrate the expected “tightening” of the parabola with decreasing temperature.

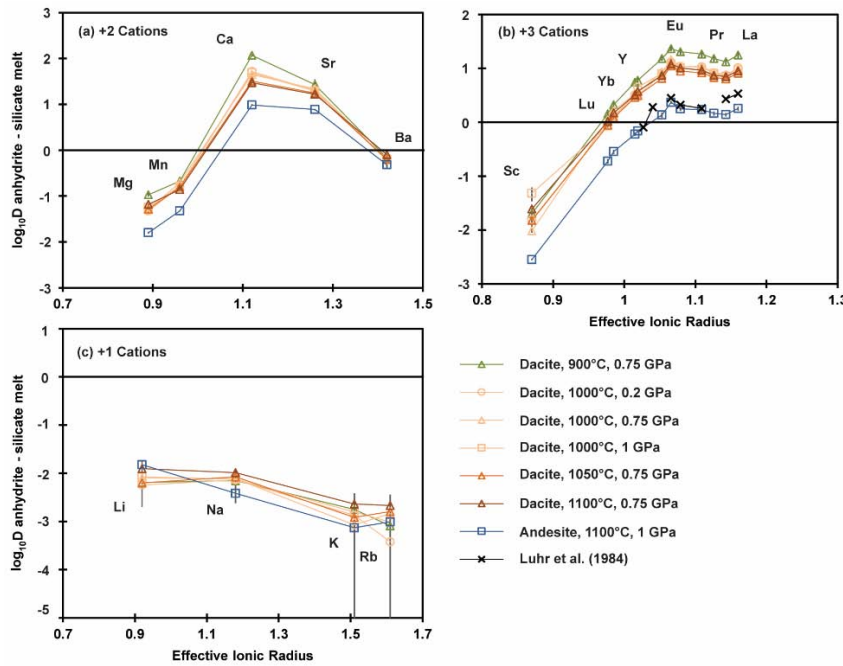


Figure 3. Anhydrite – Silicate melt partition coefficients for +2, +3 and +1 cations compared to effective ionic radius. Note that data for +2 and +3 cations can be fit by parabolas calculated from lattice strain models.

It is possible to characterise anhydrite – silicate melt partition coefficients as a function of temperature and silicate melt composition (Fig. 4) and this provides a method for estimating the crystallization temperature of natural igneous

anhydrite crystals. The crystallization temperature of anhydrite may in turn be used to estimate the bulk sulphur content of anhydrite-saturated igneous rocks, which is otherwise very challenging.

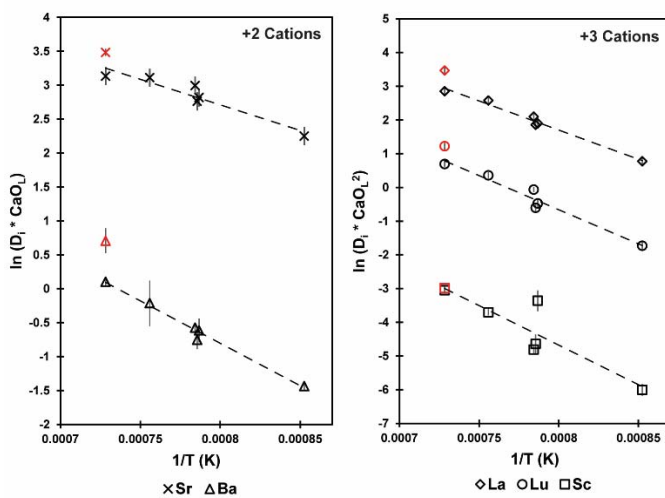


Figure 4. Anhydrite – silicate melt partition coefficients, normalised by the silicate melt CaO content (wt%, CaO_2 for +3 cations), as a function of temperature. Black symbols – dacite starting composition, red symbols – andesite starting composition. Silicate melt CaO content is used in order to account for the effect of changing melt CaO activity on exchange reactions of the form $i^{2+}_{\text{melt}} + \text{Ca}^{2+}_{\text{Anhydrite}} \leftrightarrow i^{2+}_{\text{Anhydrite}} + \text{Ca}^{2+}_{\text{melt}}$.

References

- [1] M.C. Hutchinson and J.H. Dilles (2019) *Economic Geology* 114, 143-152
- [2] I.V. Veksler et al. (2012) *Geochimica et Cosmochimica Acta* 79, 20-40

Halogen storage in nominally volatile-free minerals in the sub-cratonic lithospheric mantle

Charlotte G. Jackson and Sally A. Gibson

Department of Earth Sciences, University of Cambridge, CB2 3EQ

Background

The sub-cratonic lithospheric mantle potentially represents a significant volatile repository in the solid Earth. Theoretical studies suggest that for billions of years it has been accumulating halogens (F, Cl, Br, I) as well as sulfur, carbon and water via metasomatism linked to the percolation and reaction of fluids associated with subducting slabs or small fraction volatile-rich melts derived from the deep mantle (e.g. [1]). These metasomatised regions are associated with accessory hydrous minerals, such as apatite, amphiboles and mica, that have the potential to accommodate substantial concentrations of halogen; for example, phlogopite can hold up to 5 wt. % F. However, in the past few years it has become clear that the more abundant nominally volatile-free mantle minerals (NVFMMs; such as, olivine and pyroxene) also have the capacity to store significant volumes of halogens, in fact the entire fluorine budget of the upper mantle could be stored in nominally volatile-free phases [2]. This is **because fluorine's smaller ionic radius** makes it only moderately incompatible (compared to Cl) and allows it to substitute for OH⁻ in hydrous or nominally anhydrous phases [3].

Samples

Our study focuses on the Kaapvaal craton of southern Africa (Fig. 1). Eleven samples of peridotite from the Bultfontein kimberlite pipe, South Africa, and 8 samples from the Mothae kimberlite in Lesotho were chosen for SIMS analysis at EIMF. These samples consist of a variety of lithologies (lherzolites and harzburgites) and textures that are representative of sub-cratonic mantle. Furthermore, the xenoliths were selected because *PT* estimates indicate that they were entrained over a wide depth range in the lithospheric mantle.

Fresh grains of olivine, orthopyroxene and clinopyroxene were separated from coarse crushate and then mounted in indium (Fig. 2) and analysed for H, F and Cl by SIMS.

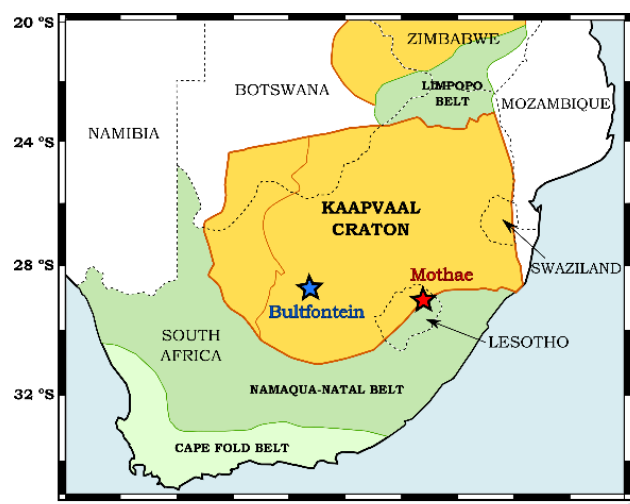


Figure 1. Map of southern Africa, showing the locations of Bultfontein and Mothae on the Kaapvaal craton interior and margin, respectively.

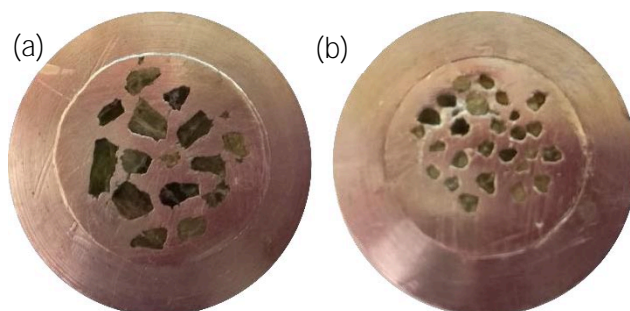


Figure 2: Two examples of the mineral separates mounted in indium: (a) Orthopyroxene; (b) Olivine. Individual crystals were picked, polished and cleaned before being pressed into indium within an aluminium disk.

Table 1. Standards used **during the analysis, those marked with a ‘*’ were used for calibration and ‘^’ were used to calibrate in May 2019.**

Standard	Olivine Analysis	Orthopyroxene Analysis	Clinopyroxene Analysis
AVL-519-4	Y*		Y
OLV-11610-10	Y	Y	Y
StA9-8.1	Y*	Y*	Y*
OPX KH03-4	Y^	Y*	
OPX116610-10	Y^	Y*	
OI-Fo	Y*		
OI-DC0212	Y		
CPX KH03-4			Y*
CPX-SC-J1			Y*
CPX-SMC31139			Y*

Results

These new SIMS analyses of mantle xenoliths entrained by the Bultfontein & Mothae kimberlites significantly expand the published dataset for volatiles, especially halogens, in nominally volatile-free minerals from sub-cratonic mantle. The spread of H₂O data in nominally-volatile-free mantle minerals analysed in this study is within the range available for the Kaapvaal and Siberian cratons [4-6]. Ortho- and clinopyroxenes are the major host of H₂O (up to 370 ppmw) in the Bultfontein and Mothae xenoliths, but olivine is found to contain the highest F contents (up to 196 ppm). By contrast, F contents in the pyroxenes range from 0 to 46 ppm. The highest F contents are observed in NVFMMs from metasomatised mantle xenoliths.

On average mantle clinopyroxene and orthopyroxene from Mothae contain lower water and higher fluorine concentrations than those from Bultfontein and suggest that there is spatial variation in the volatile content of the lithospheric mantle beneath the Kaapvaal craton. The partitioning behaviour of water between clinopyroxene and orthopyroxene is consistent with the findings of experiments, and *D* values are found to be temperature dependent. The *D* values are lower than those observed in off-craton peridotites which appears to reflect the different *PT* conditions represented by each tectonic setting.

Importance of results

We collected major element (EPMA), minor and trace element (LA-ICP-MS) and H, F and Cl (SIMS) concentrations for each mineral separate from Bultfontein and Mothae. Additional FTIR spectra have been collected in olivine and orthopyroxene in fragments from the same xenoliths. This information together with *PT* estimates has enabled a systematic investigation into the incorporation mechanisms of the volatile elements, the partitioning behaviour of volatiles between mantle minerals, the mobilisation of volatiles during metasomatism and more generally the storage of these elements in the sub-cratonic lithospheric mantle. Metasomatism is recognised as an extremely important process to introduce volatile elements to pre-existing mantle minerals, and periods of extensive metasomatic enrichment within the history of the Kaapvaal Craton are associated with significant addition of water and fluorine to the olivine, orthopyroxene and clinopyroxene. The addition of volatiles over short timescales has important implications for localised processes such as kimberlite ascent, and on large scales for the stability of the craton.

References

- [1] D McKenzie, (1989) *EPSL* 95, 53–72. [2] T Grützner et al. (2017) *GCA* 208, 160–170. [3] RW Luth (2003) *Treatise on Geochemistry* 2, 568. [4] S Demouchy and N Bolfan-Casanova (2016) *Lithos* 240–243, 402–425. [5] AH Peslier et al. (2010) *Nature* 467, 78–81. [6] AH Peslier et al. (2012) *GCA* 97, 213–246.

Origin of silica in presalt carbonates: insights from ion probe O isotopic analysis

F. Lapponi¹, I. Troth¹ & J. Craven²

¹Research Center Bergen, Equinor ASA, 5006 Sansliveien 90, Bergen, Norway

²School of GeoSciences, University of Edinburgh, Edinburgh EH9 3JW, UK

Introduction

The origin and significance of chert and silicified carbonate intervals in Cretaceous pre-salt lacustrine successions offshore Brazil and Angola is still a matter of debate and different interpretations have been provided [1-4]. The amount of silica locally increases in some discoveries and stratigraphic intervals which have important consequences in terms of matrix properties and high permeability features (fractures and vuggy systems). We performed a detailed ion probe study to characterize the oxygen isotopic composition of silica from subsurface pre-salt samples to shed insights on the diagenetic evolution of these silica-rich systems and compare with the existing published data

Silica characterisation and results

Thirty-two (32) samples were selected for the study after screening the digital images. Samples were selected to guarantee the maximum stratigraphic coverage and petrographic diversity while preserving the integrity of the samples for future work.

The samples were imported to the Equinor Research Centre in Bergen Norway and thin sections produced from the samples at the in-house facility. A digital scan of the thin sections was performed and the thin sections were screened under transmitted and reflected light optical microscope to select areas of interest for the ion probe analysis.

Forty (40) areas of 2-3 mm in diameter were identified and photographed before mini-disc samples were extracted using an ultrasonic drill. The discs were subsequently mounted on epoxy blocks together with standards, gold coated and analyzed for oxygen silica using the Cameca IMS-1270 ion microprobe at the School of Geosciences, University of Edinburgh.

The silica minerals are observed as a variety of polymorphs and crystal sizes occupying different paragenetic positions in the evolution of the rock:

1. microcrystalline quartz, few 10s of μ in diameter, usually replacing carbonate or forming a fine crystalline matrix in a carbonate framework, also referred to as '**chert**');
2. chalcedony, a fibrous cryptocrystalline form of quartz, usually showing growth banding, forming a micro-spherulitic matrix or colloform pore lining cement. It is observed as two, often alternating, forms: a length-slow form fibrous cryptocrystalline (quartzite) or length fast. The determination is performed using additional plates in the optical microscope;
3. meso- to macro-crystalline quartz cement, either as lining pores or as fracture fill.

Results of the ion probe analysis are shown diagrammatically in Figure 1 and Table 1. The data show an ample spread in values from 27 to 47 ‰ SMOW, with mean at around 38 ‰ SMOW. Similarly, a wide spread is also observed in each of the single mineral morphologies utilized for grouping the data. However, a clear decrease in the data distribution averages is observed in the **paragenetically 'late'** macro crystalline quartz cements in macro pores and fractures. An exception is the possibly early silica cemented fractures commonly completely occluded by meso-crystalline, more fibrous quartz cements (Figure 1: meso cx cement fracture). The **high $\delta^{18}\text{O}$** values from this study are not dissimilar to other data observed in the other pre-salt fields (Saller et al 2016). Silica oxygen isotopic compositions characterized by **values above 35 ‰ SMOW** are rare in the geological record and the only modern setting where silica is observed precipitating with such isotopically "**heavy**" composition is the highly evaporative Lake Magadi, in the Kenyan Rift Valley [5].

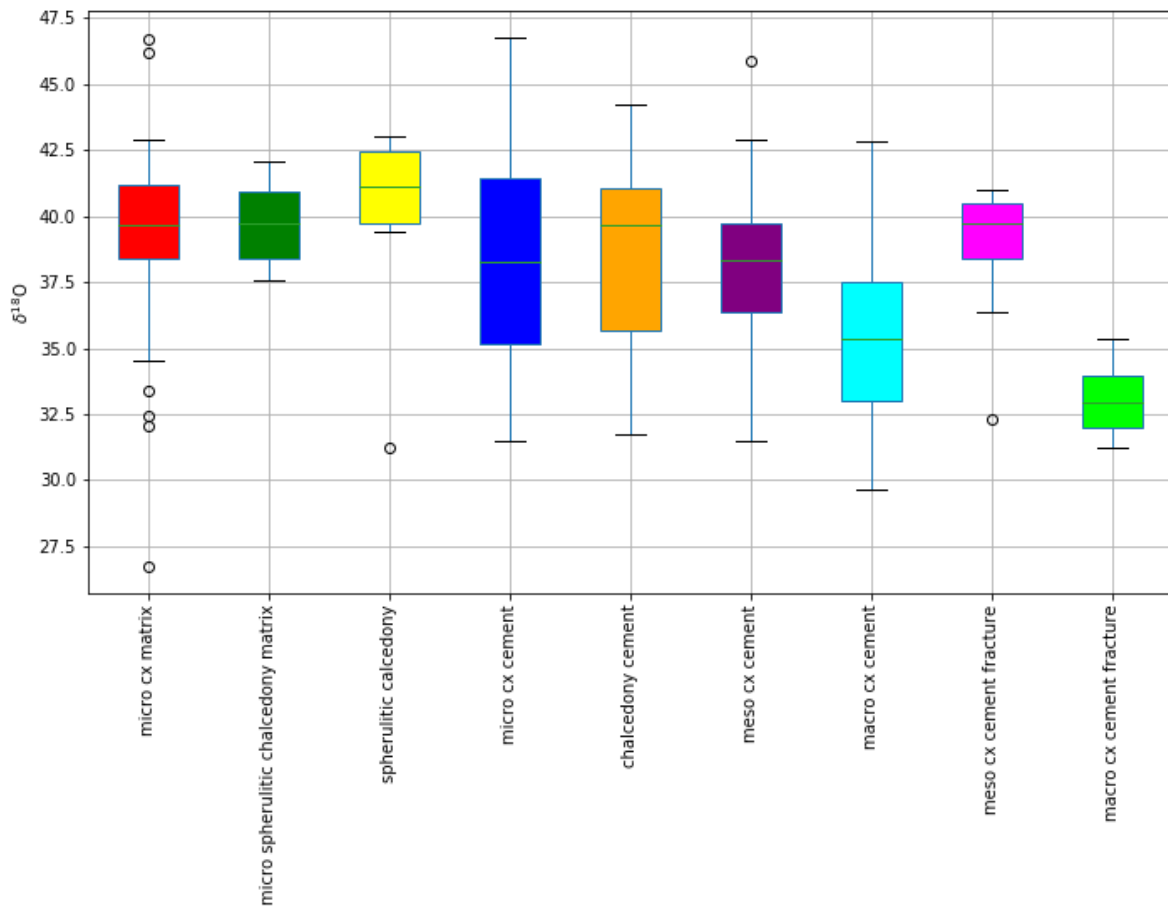


Figure 1. Boxplot showing distribution of oxygen isotopic composition of different silica morphologies ordered according their inferred paragenetic position (form left early to right late). Note the decrease on average with advancing paragenetic position. Cx = crystalline.

Table 1. Summary statistics for measured oxygen isotopic composition in ‰ SMOW

all data	chalcedony cement	macro cx cement	macro cx cement fracture	meso cx cement
count 280.000000	count 26.000000	count 81.000000	count 12.000000	count 31.000000
mean 37.702317	mean 38.507629	mean 35.395704	mean 33.043556	mean 38.142725
std 3.648114	std 3.347965	std 3.306158	std 1.357106	std 3.050030
min 26.743105	min 31.711260	min 29.638353	min 31.219702	min 31.473530
25% 35.093582	25% 35.638217	25% 33.019745	25% 32.017552	25% 36.350383
50% 38.325917	50% 39.680971	50% 35.320771	50% 32.940858	50% 38.316015
75% 40.509833	75% 41.070008	75% 37.509361	75% 33.941327	75% 39.716170
max 46.767777	max 44.246462	max 42.848864	max 35.347357	max 45.891313
meso cx cement fracture	micro cx cement	micro cx matrix	micro spherulitic chalcedony matrix	spherulitic chalcedony
count 10.000000	count 18.000000	count 78.000000	count 18.000000	count 6.000000
mean 38.765502	mean 38.504616	mean 39.418020	mean 39.751804	mean 39.762525
std 2.681558	std 4.434013	std 2.931053	std 1.414269	std 4.400316
min 32.299346	min 31.486655	min 26.743105	min 37.585151	min 31.208251
25% 38.378054	25% 35.134572	25% 38.362408	25% 38.391978	25% 39.710557
50% 39.701229	50% 38.246164	50% 39.675175	50% 39.704031	50% 41.108673
75% 40.463772	75% 41.433067	75% 41.197051	75% 40.941835	75% 42.423741
max 41.012535	max 46.767777	max 46.685737	max 42.070771	max 43.042938

References

- [1] Poros Z. et al. (2017) AAPG ACE 2017.
- [2] Saller A. et al. (2016) AAPG Bulletin, 100, 1135-1164.
- [3] Teboul P. et al. (2019) Applied Geochemistry, 100, 22-41.
- [4] Trittla J. et al. (2018) AAPG ACE 2018.
- [5] O'Neil J.R. (1973) Earth and Planetary Science Letters, 19-2, 257-266.

Using S isotope in melt inclusions to understand S cycling through subduction zones (pilot study)

T.A. Mather

Department of Earth Sciences, University of Oxford, Oxford OX1 3AN, UK

Project background

Sulfur isotopes have been proposed as potentially powerful tracers for S cycling through subduction zones. Sulfur in slab-derived fluids containing seawater ($\delta^{34}\text{S}$ sulphate $\sim 20\text{‰}$; sulphide $\sim 30\text{‰}$) differs significantly compared to mantle S ($\delta^{34}\text{S}$ $\sim -1\text{‰}$) (e.g., [1]). Although limited data exist, whole rock studies of (strongly S degassed) arc lavas find heavy $\delta^{34}\text{S}$ values compared to mantle composition. This has been used as evidence for a seawater-sulphate contribution to arc S [2,3]. More recent work finds that S in primitive Sierra Nevada cumulates is isotopically similar to mantle citing this as evidence that the contribution of slab-derived sulphate to arc lavas may not be as large as widely thought [1]. One of the issues when using whole rock compositions to test these competing models of the subduction zones S cycle is that their compositions are likely strongly influenced by shallower processes of crustal contamination and fractionation during S degassing. This makes it challenging to relate their isotopic signature to their primary melts. Efforts to correct for degassing rely on assumptions about variables such as magma oxidation state which will itself vary during the degassing [2]. To realise the power of S isotopes for tracing volatile recycling processes through subduction zones we need to access $\delta^{34}\text{S}$ compositions of arc melts containing undegassed sulfur. This necessitates the study of melt inclusions (MIs). This proposal was a proof of concept regarding the development of EIMF S isotope capabilities on MIs from arc rocks. This pilot project proved **the EIMF's potential** to make such measurements (Fig. 1) and obtained pilot data that was used in the subsequent successful proposal to NSF-NERC to fund further work at EIMF.

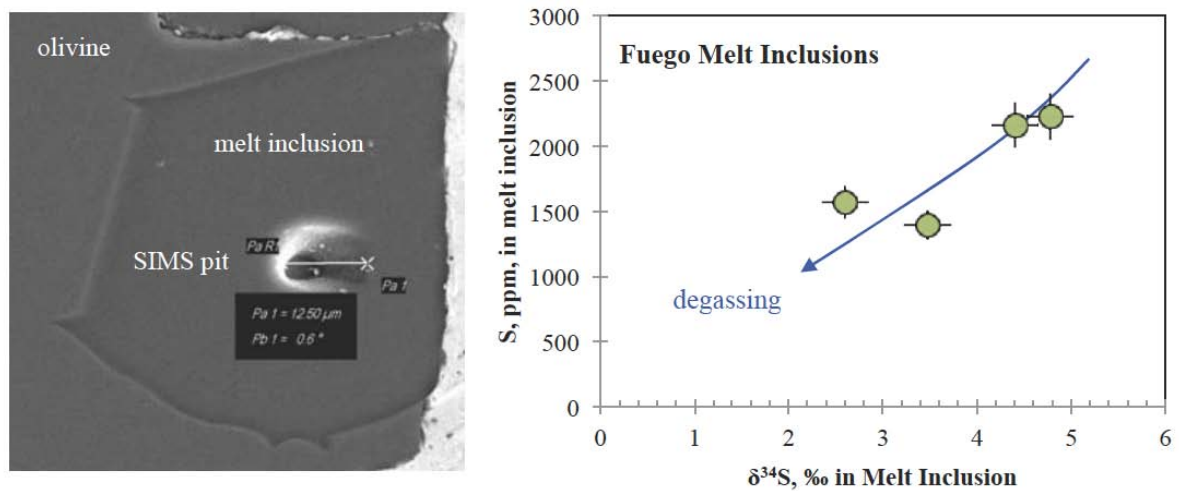


Fig. 1. Pilot data collected at EIMF. SEM image shows the 12- μm ion-probe pit within a $\sim 50\text{-}\mu\text{m}$ melt inclusion. $\delta^{34}\text{S}$ vs. concentration for four Fuego melt inclusions (error bars 8% uncertainty on electron probe S and 0.15% precision on $\delta^{34}\text{S}$ based on MORB glass replicates. [4])

Results

The pilot data are presented in Fig. 1 and are exciting for several reasons: (1) to our knowledge they are the first arc melt inclusion $\delta^{34}\text{S}$ data, (2) they show $\delta^{34}\text{S}$ values heavier than MORB, which cannot derive simply from the background arc mantle, as (3) at this f_{O_2} degassing only serves to lower the $\delta^{34}\text{S}$,

so the heavy values appear to characterize the initial magma compositions and **(4) the positive $\delta^{34}\text{S}$** is surprising given that the sediments subducting into the Central America trench appear dominated by pyrite [5], **which typically has light $\delta^{34}\text{S}$** , although there are barite-rich domains too which would be **expected to have heavy $\delta^{34}\text{S}$** .

References

- [1] Lee et al. (2018) Earth and Planetary Science Letters 500, 76-85
- [2] de Hoog et al. (2001) Earth and Planetary Science Letters 189, 237-252
- [3] Alt et al. (1993) Earth and Planetary Science Letters 119, 477-494
- [4] Fiege et al. (2014) Geochimica et Cosmochimica Acta 142, 501-521.
- [5] Solomon and Kastner. (2012) Geochimica et Cosmochimica Acta 83, 110-124.

The effect of rapid crystal-growth on trace element partitioning in plagioclase and clinopyroxene

A. McCarthy, J. Ryker & J. Blundy

¹School of Earth Sciences, University of Bristol, Bristol, BS8 1RJ, UK

Introduction

Partition coefficients describing equilibrium partitioning of trace elements between silicate melts and crystals are widely used as a geochemical tool to infer residence timescales of individual crystals, melt composition and/or open system assimilation-fractional crystallization. However, shallow magmatic reservoirs, melt extraction zones, lava lakes, dykes and erupted volcanic products are prone to disequilibrium, rapid crystal growth up to several orders of magnitude faster than equilibrium crystallization. Thus, the possibility of disequilibrium fractionation during rapid crystal growth in shallow magmatic environments might be extensive, with the consequence that trace element variations in single crystals might not faithfully reflect the composition of the melt according to “traditional” (i.e. equilibrium) partition coefficients.

To target such a process, we focused on a unique suite of dry, plagioclase-phyric mid-ocean-ridge basalts (MORB) from the South China Sea. These lava flows have homogeneous plagioclase phenocrysts and glass composition over a hundred meter thick interval. However, rapid cooling conditions within quenched pillow lobes leads to acicular and swallow-tail habits with bow-fan and stellate arrangements of plagioclase and clinopyroxene (Fig. 1). The interior of thick flows are composed of coarser

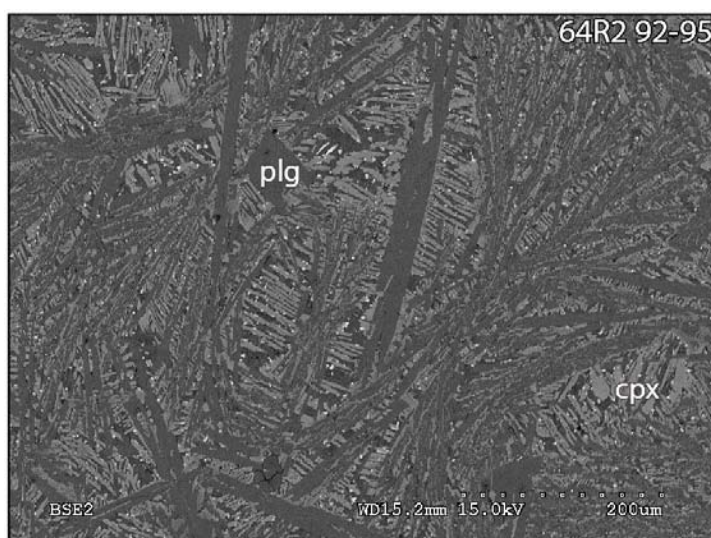


Figure 1. Interior section of a MORB pillow lava showing rapid-growth textures of plagioclase and clinopyroxene. Swallow-tail plagioclase in elongated clinopyroxene show a shift towards elevated MgO, FeO and Al₂O₃, Na₂O and TiO₂ respectively in rapid-growth conditions.

grained and blocky euhedral plagioclase and clinopyroxene showing normal chemical zoning, consistent with slower cooling conditions. Extensive microprobe analysis (>1000 analysis) has shown that clinopyroxene show significant shifts to higher Al₂O₃, TiO₂, Na₂O and lower Mg# as cooling rates, and thus growth rates, increase. Plagioclase shows a similar increase in MgO and FeO at near constant Anorthite content with increasing cooling rate. Thus, a combination of LA-ICP-MS analysis of coarse grained plagioclase and clinopyroxene combined to SIMS analysis of fine grained, disequilibrium plagioclase and clinopyroxene would allow us to constrain the effect of changes in cooling rate on trace element uptake in both minerals.

Results

Our analytical session at the SIMS Facility at Edinburgh used low beam currents (~0.02 nA) to achieve a <2μm spot size of both plagioclase and clinopyroxene. Extensive analysis of plagioclase by SIMS has confirmed our initial results obtained by microprobe indicating that increasing cooling rates leads to increasing MgO and FeO at near-constant Anorthite abundance (Fig. 2). However, we also show that neither Li, Sr, Ba, TiO₂ (Fig. 2) are affected by such sudden shifts in growth rates as all elements fully overlap in plagioclase from different cooling rates. Clinopyroxene on the other hand, show nearly an

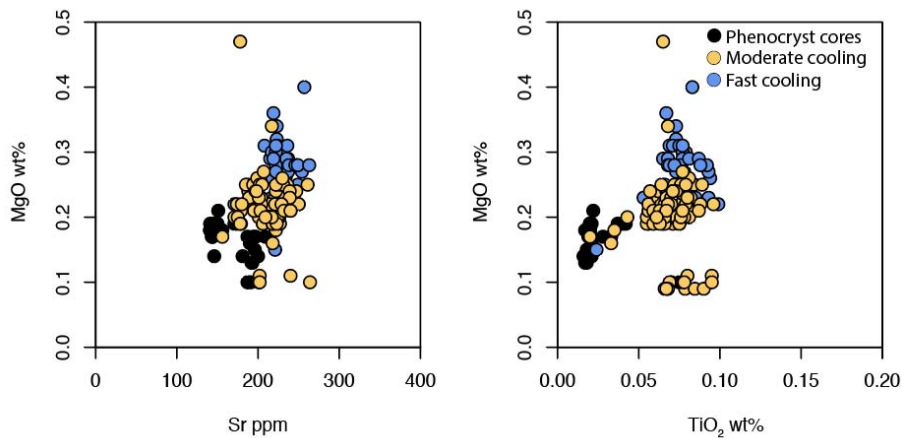


Figure 2. SIMS analysis of plagioclase show that increasing cooling rate leads to higher MgO (blue dots) and FeO, whereas Sr and TiO₂ remain constant.

order of magnitude of increase in trace element abundances with increasing cooling rate (Fig. 3), leading to clinopyroxene enriched in Ce, Y, Zr, Sr and V which coincide with increasing Al₂O₃, TiO₂ and Na₂O.

Discussion

We have been able to combine extensive microprobe, LA-ICP-MS and SIMS analysis to target the change in mineral chemistry as a function of cooling rate. As a result of the use of the analytical capabilities of the NERC facility at Edinburgh we have produced an extensive and unique dataset highlighting extreme heterogeneity in erupted volcanic products. Crucially, we show that clinopyroxene in particular is sensitive to growth rates, whereas plagioclase chemistry, aside from MgO and FeO, does not seem particularly sensitive to growth rates. This dataset shows that Sr and Ba partitioning in plagioclase might not be too sensitive to growth rates, implying that the use of equilibrium partitioning might still be suitable to infer residence timescales of shallow volcanic phenocrysts. We are currently developing a numerical model to constrain the evolution of trace element uptake in plagioclase as a function of growth rates to target the evolution of MgO and FeO in plagioclase. This study has several implications regarding the study of erupted volcanic products (tephra, ash, scoria, lava flows) which are generally used to infer P-T-fO₂-H₂O conditions of magmatic eruptions prior to volcanic eruptions.

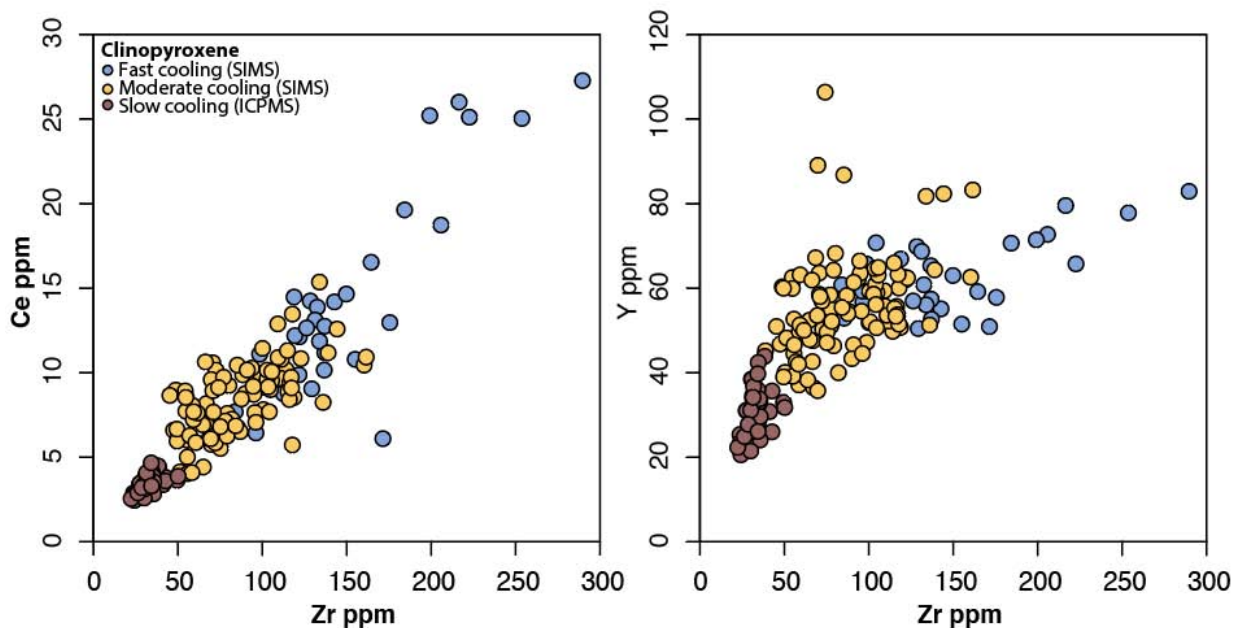


Figure 3. LA-ICP-MS (red) and SIMS analysis (yellow, blue) of clinopyroxene as a function of cooling rate. Clinopyroxene show a marked increase in trace element abundances (Zr, Ce, Y) as a consequence of increasing cooling rate.

Sulfur isotope evidence of ancient subsurface life: implications for Mars

S. McMahon^{1,2}, J. Parnell³ & P. Reekie^{1,2}

¹School of GeoSciences, University of Edinburgh, Edinburgh EH9 3JW, UK

²UK Centre for Astrobiology, School of Physics & Astronomy, University of Edinburgh, EH9 3FD, UK

³School of Geosciences, University of Aberdeen, King's College, Aberdeen, AB24 3UE, UK

Introduction

Calcium sulfate mineral veins cross-cut ancient sedimentary rocks at multiple localities on Mars and are of astrobiological interest as evidence of subsurface aqueous fluid transport. However, their potential to preserve biosignatures is unknown. We found pyrite embedded in the margins of a fibrous gypsum vein of probable Cenozoic emplacement age in Permian lacustrine mudrocks from Cumbria. The complex, interfingering morphology of the pyrite–gypsum interface suggests that the pyrite grew authigenically in porosity created when reducing fluids dissolved gypsum at the vein margins. Spatially resolved ion microprobe (SIMS) measurements of **pyrite sulfur isotope composition ($\delta^{34}\text{S}$)** were obtained using the Edinburgh NERC IMF in order to test whether the pyrite records microbial sulfate reduction, which, in contrast to abiotic (thermochemical) sulfate reduction, produces sulfide characterised by $\delta^{34}\text{S}$ values several **tens of ‰ more negative than the precursor sulfate**.

Materials and methods

The bedding-parallel mudstone-hosted antitaxial fibrous gypsum vein we analysed was collected in hand samples underground *in situ* from the Kirkby Thore gypsum mine, which accesses the Eden Shales Formation of the Cumbrian Coast Group in the Vale of Eden Basin, Cumbria, NW England. The sample was mounted in epoxy for SIMS analysis and, after some trial and error, ground down sufficiently to prevent problematic dehydration outgassing under vacuum.

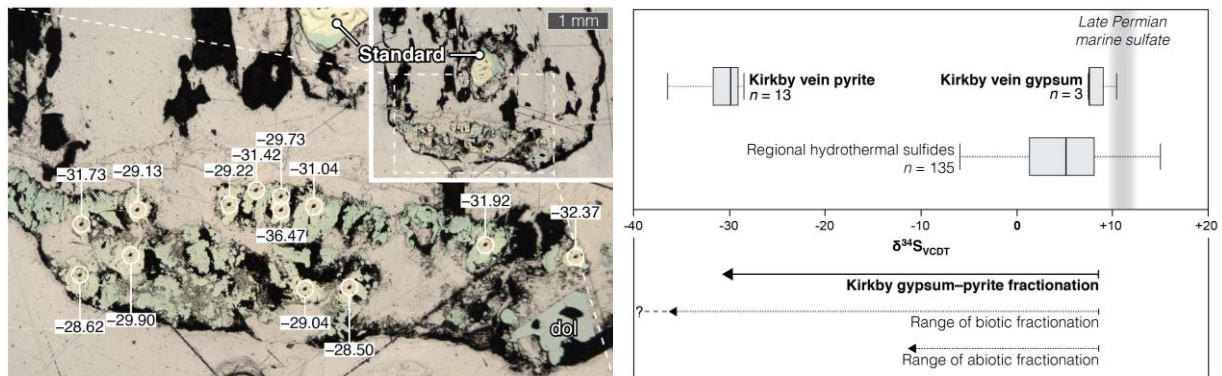


Figure 1. Left: Reflected light image of mounted sample showing pyrite (greenish) and dark pits made by the ion beam; measured $\delta^{34}\text{S}$ value are indicated. “dol” = dolomite crystal. Right: Measured values (“Kirkby vein pyrite”) in context, with inferred magnitude of fractionation from the original sulfate $\delta^{34}\text{S}$ indicated. Sulfur isotope compositions for the gypsum itself and from hydrothermal sulfide veins in NW England were previously published [1].

Results and implications

The pyrite sulfur isotope composition was found to be **consistently very light (mean $\delta^{34}\text{S}_{\text{VCDT}} = -30.7$ ‰; n = 13, Fig. 1)**. Comparison with the sulfate in the gypsum ($\delta^{34}\text{S}_{\text{VCDT}} = +8.5$ ‰; data obtained previously) indicates strong fractionation. We infer from this and from other evidence (close association between the pyrite and embedded organic matter; low temperature burial history of host rock) that the pyrite is indeed microbial in origin and therefore that sulfate veins can incorporate biosignatures formed in the subsurface. In principle, similar subsurface biosignatures could be detectable in Martian veins, particularly if they were selected to be returned to Earth for SIMS analysis.

The presence of preserved organic matter adds to the case that such veins could be an attractive target for analysis on Mars.

References

[1] J. Armstrong, J. Parnell, A.J. Boyce, A.J. and L.A. Bullock (2020). *Ore Geology Reviews* **116**: 103207.

Appendix: analytical details

Sulfur isotopes (^{32}S and ^{34}S) were analysed as S^- ions produced by bombardment of the target by a ~ 1 nA, $^{133}\text{Cs}^+$ primary beam accelerated at +10 kV resulting in a net impact energy of 20 keV at the sample surface. Secondary ions were accelerated at -10 kV and analysed at a mass resolution sufficient to resolve molecular interference by $^{33}\text{S}^1\text{H}$ and $^{32}\text{S}^1\text{H}_2$ on the $^{34}\text{S}^-$ peak. An energy window of 40 eV was used. After pre-sputtering for 30 s, automated secondary ion beam alignment was performed using the DT_{xy} deflection plates to centre the beam in the mass spectrometer field aperture (2,500 μm) and entrance slit (90 μm) positions. Count rates were typically $\sim 2 \times 10^8$ cps of ^{32}S and $\sim 9 \times 10^6$ cps of ^{34}S . The total acquisition time was 100 s comprising of 20 cycles, split into two blocks of 10, with each cycle comprising of a 5 s counting period. A single ~ 4 -min analysis (including 30 s pre-sputtering time and beam centring routines) resulted in an internal error of $< 0.25\%$.

Publications

McMahon, S., Parnell, J., & Reekie, P. Mars-analogue calcium sulfate veins record evidence of ancient subsurface life. *Astrobiology*: Accepted pending minor revisions.

Sulfur isotope evidence of ancient subsurface life: implications for Mars

S. McMahon^{1,2}, J. Parnell³ & P. Reekie^{1,2}

¹School of GeoSciences, University of Edinburgh, Edinburgh EH9 3JW, UK

²UK Centre for Astrobiology, School of Physics & Astronomy, University of Edinburgh, EH9 3FD, UK

³School of Geosciences, University of Aberdeen, King's College, Aberdeen, AB24 3UE, UK

Introduction

Calcium sulfate mineral veins cross-cut ancient sedimentary rocks at multiple localities on Mars and are of astrobiological interest as evidence of subsurface aqueous fluid transport. However, their potential to preserve biosignatures is unknown. We found pyrite embedded in the margins of a fibrous gypsum vein of probable Cenozoic emplacement age in Permian lacustrine mudrocks from Cumbria. The complex, interfingering morphology of the pyrite–gypsum interface suggests that the pyrite grew authigenically in porosity created when reducing fluids dissolved gypsum at the vein margins. Spatially resolved ion microprobe (SIMS) measurements of **pyrite sulfur isotope composition ($\delta^{34}\text{S}$)** were obtained using the Edinburgh NERC IMF in order to test whether the pyrite records microbial sulfate reduction, which, in contrast to abiotic (thermochemical) sulfate reduction, produces sulfide characterized by $\delta^{34}\text{S}$ values several tens of ‰ more negative than the precursor sulfate.

Materials and methods

The bedding-parallel mudstone-hosted antitaxial fibrous gypsum vein we analysed was collected in hand samples underground *in situ* from the Kirkby Thore gypsum mine, which accesses the Eden Shales Formation of the Cumbrian Coast Group in the Vale of Eden Basin, Cumbria, NW England. The sample was mounted in epoxy for SIMS analysis and, after some trial and error, ground down sufficiently to prevent problematic dehydration outgassing under vacuum.

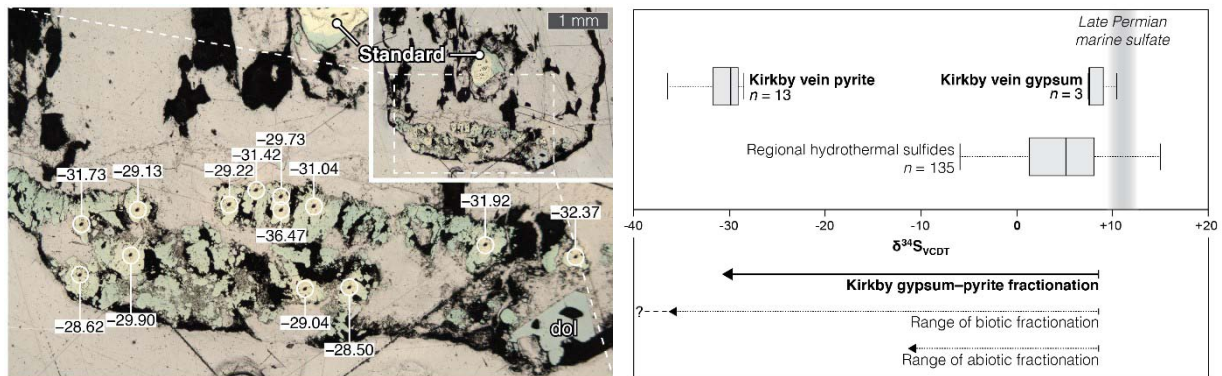


Figure 1. Left: Reflected light image of mounted sample showing pyrite (greenish) and dark pits made by the ion beam; measured $\delta^{34}\text{S}$ value are indicated. “dol” = dolomite crystal. Right: Measured values (“Kirkby vein pyrite”) in context, with inferred magnitude of fractionation from the original sulfate $\delta^{34}\text{S}$ indicated. Sulfur isotope compositions for the gypsum itself and from hydrothermal sulfide veins in NW England were previously published [1].

Results and implications

The pyrite sulfur isotope composition was found to be **consistently very light** (mean $\delta^{34}\text{S}_{\text{VCDT}} = -30.7$ ‰; $n = 13$, Fig. 1). Comparison with the sulfate in the gypsum ($\delta^{34}\text{S}_{\text{VCDT}} = +8.5$ ‰; data obtained previously) indicates strong fractionation. We infer from this and from other evidence (close association between the pyrite and embedded organic matter; low temperature burial history of host rock) that the pyrite is indeed microbial in origin and therefore that sulfate veins can incorporate biosignatures formed in the subsurface. In principle, similar subsurface biosignatures could be detectable in Martian veins, particularly if they were selected to be returned to Earth for SIMS analysis.

The presence of preserved organic matter adds to the case that such veins could be an attractive target for analysis on Mars.

References

[1] J. Armstrong, J. Parnell, A.J. Boyce, A.J. and L.A. Bullock (2020). *Ore Geology Reviews* **116**: 103207.

Appendix: analytical details

Sulfur isotopes (^{32}S and ^{34}S) were analysed as S^- ions produced by bombardment of the target by a ~ 1 nA, $^{133}\text{Cs}^+$ primary beam accelerated at +10 kV resulting in a net impact energy of 20 keV at the sample surface. Secondary ions were accelerated at -10 kV and analysed at a mass resolution sufficient to resolve molecular interference by $^{33}\text{S}^1\text{H}$ and $^{32}\text{S}^1\text{H}_2$ on the $^{34}\text{S}^-$ peak. An energy window of 40 eV was used. After pre-sputtering for 30 s, automated secondary ion beam alignment was performed using the DT_{xy} deflection plates to centre the beam in the mass spectrometer field aperture (2,500 μm) and entrance slit (90 μm) positions. Count rates were typically $\sim 2 \times 10^8$ cps of ^{32}S and $\sim 9 \times 10^6$ cps of ^{34}S . The total acquisition time was 100 s comprising of 20 cycles, split into two blocks of 10, with each cycle comprising of a 5 s counting period. A single ~ 4 -min analysis (including 30 s pre-sputtering time and beam centring routines) resulted in an internal error of $< 0.25\%$.

Chlorine Isotope fractionation during degassing of lunar magmas

N.J. Potts & G.D. Bromiley

School of GeoSciences, University of Edinburgh, Edinburgh EH9 3JW, UK

Rationale

The Moon formed following collision of a Mars-sized proto-planet with the newly formed Earth approx. 4.4 billion years ago. In contrast to Earth, the Moon has remained relatively unprocessed by geological activity since this time, and provides insight into the early Earth-Moon system. An example of this is constraining the origin of Earth's water. **Water sustains life on Earth and has a key role in many geological processes, from melting and volcanism to mantle deformation and plate tectonics.** The presence of trace amounts of water (or H) in lunar samples implies that water was delivered to the Earth during its accretion, either before or just after the Moon-forming impact. Other volatiles provide additional insight. Chlorine is commonly used to trace hydrous processes on Earth and is readily detected in lunar samples. Proportions of its two stable isotopes, ^{35}Cl and ^{37}Cl , are also a useful chemical fingerprint. In fact, the ratio of ^{35}Cl to ^{37}Cl in lunar samples $\delta^{37}\text{Cl}$ (‰) = $[(^{37}\text{Cl}/^{35}\text{Cl}_{\text{sample}}/^{37}\text{Cl}/^{35}\text{Cl}_{\text{SMOC}})-1] \times 1000$, where SMOC=standard mean ocean chloride) is unique in the solar system. **In terrestrial rocks $\delta^{37}\text{Cl}$ clusters around 0‰, and in undifferentiated meteorites (the building blocks of rocky planets) varies from -4 to +10‰. However, in lunar rocks $\delta^{37}\text{Cl}$ varies from -4 to +40‰ or more. There is intense debate on the cause of this unique Cl fingerprint.** It may represent a high temperature process in which ^{35}Cl was preferentially lost from the Moon during its formation, during later magmatic activity, or may be due to a later metasomatic process. The presence of Cl in lunar rocks constrains delivery of volatiles to the early Earth-Moon system, but suggests that a significant proportion of these volatiles were lost from the Moon. Therefore, determining how and **when Cl was lost is key to understanding the origin of Earth's water.**

All models for Cl isotopic fractionation are reliant on degassing mechanisms that are theorised but experimentally unconstrained. Therefore, we performed short duration, high-temperature degassing experiments in model basaltic system at 1500°C, under correspondingly reducing conditions, to constrain the extent of, and mechanisms for, chlorine degassing. Experiments were performed in both H-free, H-bearing and Zn-bearing systems. Following experiments, major element chemistry of all samples was determined by electron probe microanalysis (EPMA), and Cl isotopic composition by SIMS using the Cameca 1270 ion microprobe. Basaltic and silicic glass standards were kindly donated to this project by Magali Bonifacie and Jamie Barnes. These glasses span a range of Cl abundance and isotopic composition, while also allowing major composition matrix effects to be addressed.

Results and Discussion

As shown in Fig. 1a, degassing of Cl should result in preferential loss of lighter ^{35}Cl , and elevation of $\delta^{37}\text{Cl}_{\text{magma}}$. In terrestrial systems, this kinetic fractionation is counter-balanced by HCl degassing, which enriches magma in ^{35}Cl [1]. This explains why little fractionation of Cl occurs on Earth. In contrast, metal chloride degassing in H-poor systems, such as during mare volcanism on the Moon, should further elevate $\delta^{37}\text{Cl}_{\text{magma}}$, explaining Cl isotope data from the lunar sample suite [2-4]. EMPA data from our experiments indicate that Cl is lost as ZnCl_2 and, to a lesser extent, FeCl_2 . Presence of Zn greatly enhances Cl loss and Cl fractionation (Fig. 1b). However, importantly, observed fractionation of Cl is significantly less than predicted by ideal Rayleigh fractionation (blue line, Fig. 1b). We also note that the presence of H enhances Cl loss, but results in greater, rather than less, Cl isotope fractionation, counter to previous assertions [1-4]. It is likely that fast H diffusion (Fig. 1c) means that FeCl_2 or ZnCl_2 degassing always dominates, resulting in a consistent pattern of Cl isotope fractionation. This casts doubt on the ability of HCl to counter kinetic fractionation of Cl during magmatic processes.

We have successfully demonstrated a protocol for in-situ analysis of Cl isotope signatures in experimental run products at the EIMF. First results allow for the testing of proposed models for high

temperature Cl isotopic fractionation during degassing. Results suggest that previous models of Cl degassing and isotopic fractionation in lunar systems are unreliable. Experiments cast doubt on the ability of magmatic degassing (Cl loss during mare volcanism) to explain Cl isotopic systematics for the Moon. Intriguingly, results also cast doubt on explanations for a lack of Cl isotopic fractionation on Earth. We are currently performing an additional series of experiments to more accurately constrain fractionation of Cl during progressive degassing in H-free and H-bearing atmospheres, including experiments at varying temperatures, to test proposed models of lunar degassing (volatile loss during moon formation, during lunar magma ocean solidification and during later mare volcanism). Based on these results, we have also applied for support for a larger experimental study to provide new insight into Cl isotope fractionation during Moon formation and lunar magmatism aimed at determining causes for the moons unique Cl isotopic signature.

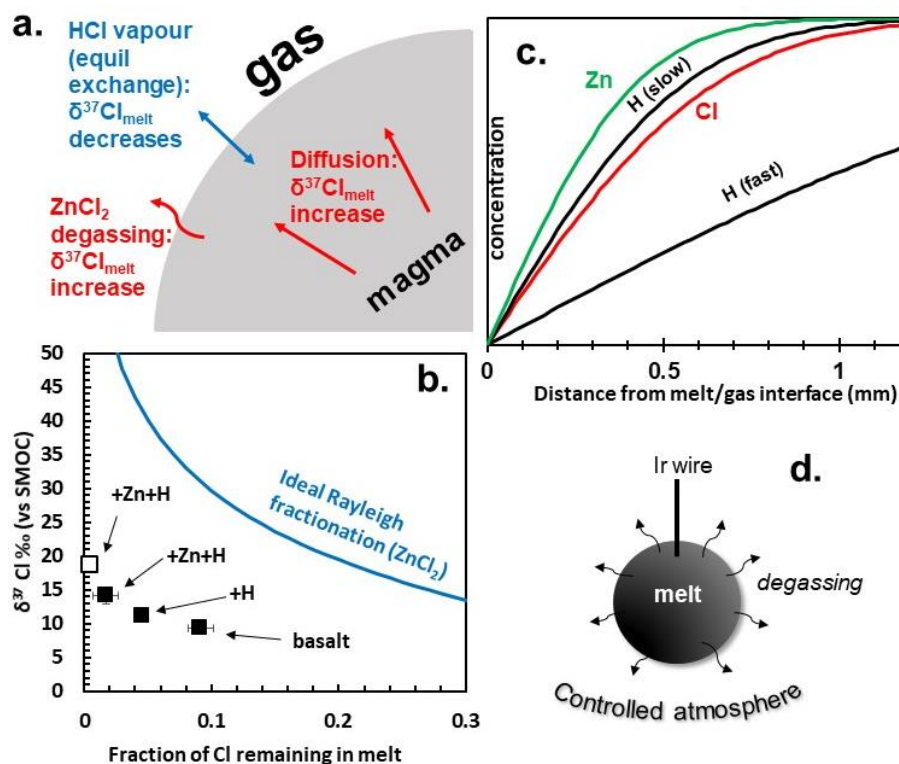


Figure 1. Mechanisms for Cl fractionation during magma degassing in H-poor and H-rich systems. b. Experimental results on Cl degassing and fractionation in a model lunar basaltic system, showing the change in $\delta^{37}\text{Cl}$ during degassing (filled=4 mins, open=6 mins). Blue line is a modelled Rayleigh fractionation curve based on ZnCl_2 , as indicated by EMPA data here. Experimental setup shown in (d). Extent of degassing is consistent with modelled Zn and Cl diffusion (c).

Acknowledgement

This work was conducted as part of NERC NE/M000346/1 “The Volatile Legacy of the Early Earth” (Bromiley PI), and as part of the wider Habitable Planets NERC consortium.

References

- [1] Sharp, Z. D., Shearer, C. K., McKeegan, K. D., Barnes, J. D. & Wang, Y. Q. The Chlorine Isotope Composition of the Moon and Implications for an Anhydrous Mantle. *Science*. 329, 1050–1053 (2010).
- [2] Boyce, J. W. et al. The chlorine isotope fingerprint of the lunar magma ocean. *Sci. Adv.* 1, (2015).
- [3] Barnes, J. J., Franchi, I. A., McCubbin, F. M. & Anand, M. Multiple reservoirs of volatiles in the Moon revealed by the isotopic composition of chlorine in lunar basalts. *Geochim. Cosmochim. Acta* 266, 144–162 (2019).
- [4] Stephant, A. et al. The chlorine isotopic composition of the Moon: Insights from melt inclusions. *Earth Planet. Sci. Lett.* 523, (2019).

Constraining the volatile history of the Campanian Ignimbrite eruption

V. Smith¹, M. Humphreys², E. Fallon³ & R. Brooker³

¹Research Laboratory for Archaeology, University of Oxford, Oxford OX1 3TG, UK

²Department of Earth Sciences, Durham University

³School of Earth Sciences, University of Bristol, Wills Memorial Building, Bristol BS8 1RJ, UK

Introduction

The Campanian Ignimbrite from Campi Flegrei caldera (Italy) was the largest eruption in Europe in the last 200 ka. It ejected >300 km³ of magma, covering regions east of the vent in Plinian fallout and the pyroclastic density current (PDC) deposits spread over more than 10,000 km² and climbed 1600 m-high mountains >40 km away. The PDCs appear to have been unusually mobile implying that they were dilute and contained large amounts of gas. The objective of this study is to determine the source of the gas, e.g. hydrothermal system or seawater, and establish whether volcanoes located close to large bodies of water are more likely to produce these incredibly dangerous PDCs.

A main aim of our study is to constrain the volatile history of the CI magmatic system. We are building upon our previous work at Campi Flegrei, which used apatite data to reveal that the systems of the smaller post-15 ka eruptions remain volatile undersaturated until shortly before the eruption^[1,2]. Using the volatile element compositions of apatite inclusions and microphenocrysts it is possible to obtain temporal information on the volatile history of the magma. In December 2019, we analysed major, trace and volatile elements in a representative suite of apatite inclusions within phenocrysts (mostly clinopyroxene) and microphenocrysts from samples taken through the CI eruption stratigraphy. Samples from the Plinian fallout and three different PDC units (in stratigraphic order)^[3]: Lower Pumice Flow (LPF) Breccia Museo (BM), and the Upper Pumice Flow (UPF) were analysed. Glass compositions of these samples indicate that they represent both of the distinct magmas that were tapped during the CI eruption; the first magma had higher dissolved Cl and F in the melt on eruption and was cooler than Magma 2 that was tapped later in the eruption^[3,4].

Results

The CI apatite inclusions and microphenocrysts were analysed on the Cameca-7f with a 18 keV net impact energy (13 keV primary and 5 keV secondary) **¹⁶O– primary ion beam**. The instrument had not been previously used to analyse apatite. Most of the apatite crystals were analysed using 20 nA current that corresponded to a beam size of 10 microns. The current was reduced to 500 pA to decrease the beam to around 2 micron and allow smaller apatite crystals and zones within some crystals to be analysed. The beam was rastered over an area, 20 microns when running at 20 nA and 5 microns at 500 pA, for 3 mins prior to the analysis to remove the surface layer and any potential contamination. Counts on the following elements: ¹H, ¹²C, ¹⁶O, ¹⁶O¹H, ¹⁹F, ²³Na, ²⁵Mg, ³⁰Si, ³¹P, ³²S, ³⁵Cl, and ⁴⁴Ca were collected using the 20 nA routine, and all except ¹²C were collected using the smaller beam size (500 pA) as the counts were too low. The ⁴⁴Ca was used as the internal standard for all analyses, and Ca contents were determined using a wavelength-dispersive electron microprobe at the University of Oxford. The apatite H₂O, CO₂, F and Cl concentrations were determined by generating calibration curves using the normalised (to ⁴⁴Ca) volatile counts collected on a range of natural and synthetic apatite standards^[5]. In addition, both ¹H and ¹⁶O¹H were analysed to establish H₂O contents and data from both are in perfect agreement. Data obtained using the different routines (20 nA and 500 pA) on the same sample are indistinguishable (Fig. 1d).

Our ionprobe data from the apatite crystals show two distinct compositional groups: a Cl-rich group with 0.89 ± 0.10 wt% Cl, 1.14 ± 0.15 wt% H₂O and 2.23 ± 0.14 wt% F (*n*=75); and a F-rich group with 3.04 ± 0.23 wt% F (*n*=65) and lower H₂O (0.69 ± 0.19 wt%) and Cl (0.36 ± 0.05 wt %) (Fig. 1a, b). There are temporal variations in X_{OH} within the groups, and particularly in the F-rich group, but X_F/X_{Cl} remains constant in each. The Plinian fall apatite inclusions plot separately from the microphenocrysts in both groups, with the microphenocrysts displaying lower X_{OH} contents relative to X_{Cl} and X_F (Fig. 1c). We have run some preliminary models of these data using the constraints we have on the melts erupted.

The observed trends are consistent with volatile undersaturated crystallisation within two different magmas (Fig. 1a, b). We will interrogate the results of the models over the next few months to see whether the partition, distribution, and exchange coefficients required to fit the trends are reasonable. There are no variations in volatile concentrations across apatite inclusions or microphenocrysts, even those that appeared zoned in back-scattered electron or cathodoluminescence images, further confirmation that volatiles diffusively re-equilibrate relatively quickly within apatite.

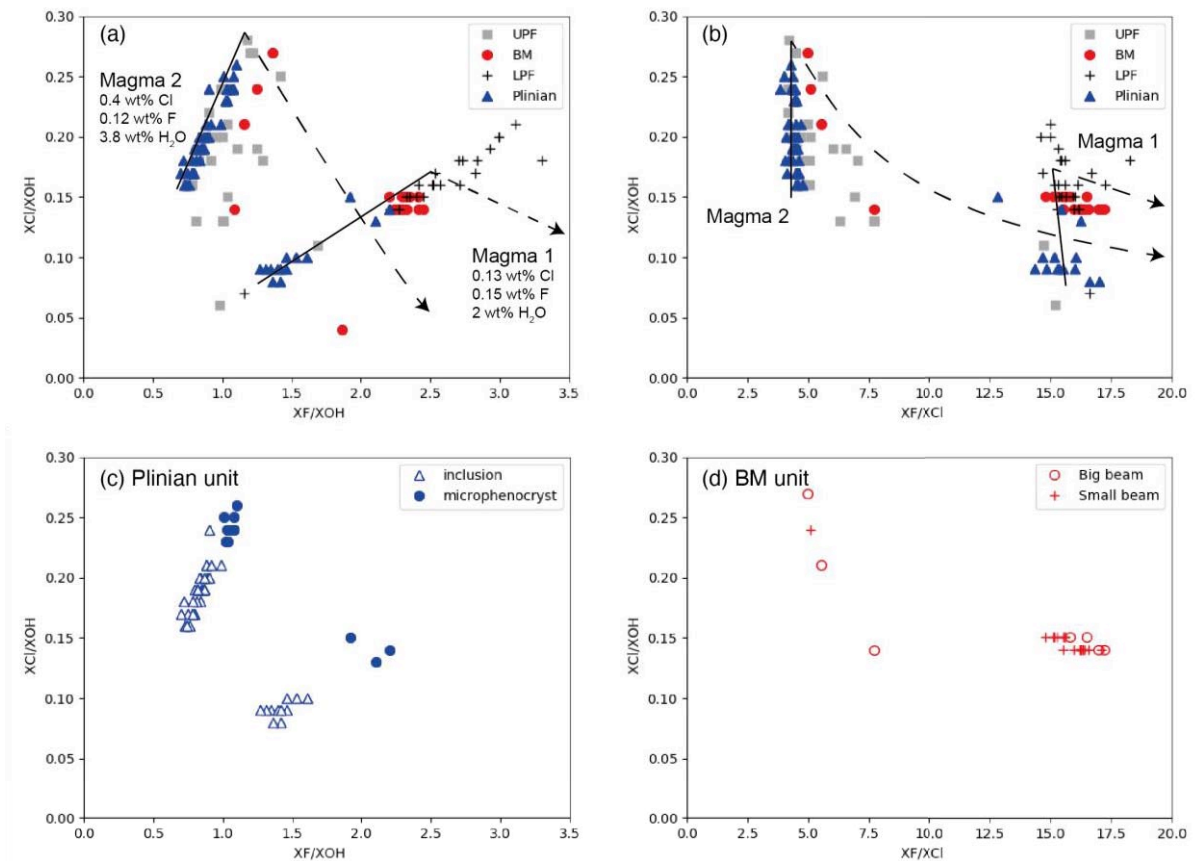


Figure 1. (a) and (b) Apatite volatile compositions of inclusions and microphenocrysts from various Cl units. Note that there is a Cl-rich (lower XF/XCl) and a F-rich group. Preliminary modelled compositional trajectories during volatile undersaturated (solid lines) and volatile saturated (dashed) crystallisation of different magmas are shown and initial melt volatile contents used to fit the model are stated. (c) Volatile compositions of apatite in the Plinian fall unit showing that the microphenocrysts have lower XOH contents. (d) Volatile compositions of microphenocrysts from the Breccia Museo sample collected using the different beam currents (big beam: ~10 micron at 20 nA, small beam: ~2 micron at 500 pA).

Further work

We have not used all our analytical time and intend to analyse more apatite inclusions in late crystallising phases (biotite and sanidine) to further constrain the temporal trends. We will carry out further modelling on these apatite data to more accurately constrain the volatile history of the magmas. These apatite data will be integrated other petrological datasets, including melt inclusion analyses that are being collected by USA collaborators on this NSFGE0-NERC project. By coupling these data with new PDC volume estimations, we will be able to provide detailed information on the amount of dissolved and exsolved gas in the magmatic system at the time of the eruption.

References

- [1] M.J. Stock et al. (2016) *Nature Geoscience* 9, 249-255.
- [2] M.J. Stock et al. (2018) *Journal of Petrology* 59, 2463–2492.
- [3] V.C. Smith et al. (2016) *Bulletin of Volcanology* 78, 45.
- [4] S. Signorelli et al., (2001) *Contributions to Mineralogy and Petrology* 140: 543-553.
- [5] R.A. Brooker et al. (in preparation) *American Mineralogist*.

Investigating the water content of diamond inclusions: analysis of trace element concentration of olivine diamond inclusions and olivine synthesised in equilibrium with saline-rich fluid

N. Tabassum, S. C. Kohn, R. Brooker, G. Bulanova, C. B. Smith.

School of Earth Sciences, University of Bristol, Wills Memorial Building, Bristol, BS8 1RJ, UK

Scientific background

Quantification of the water concentration of the Earth's interior has been a long-standing challenge in geology. The water content of nominally anhydrous mantle minerals dictates their mineralogical properties, which in turn dictates the processes that occur in the mantle. Previous studies that attempt to quantify mantle water concentrations depend on indirect geophysical studies or relatively-direct geochemical studies on mantle xenoliths.

Diamonds can contain trapped inclusions of nominally anhydrous minerals (NAMs). Ultrapotassic rocks transport diamonds from the mantle: lithospheric diamonds originate between 140 – 225 km and sublithospheric diamonds can transport diamonds with inclusions that indicate lower mantle lithology [1]. Moreover, lithospheric diamond inclusions indicate ages of up to 3.5 Ga [2]. Thus, diamonds allow direct analysis of the deepest samples of the mantle and the inert diamond host allows the inclusions to preserve their geochemistry at the time of entrapment.

Analysis of water in diamond inclusions is currently very limited: only a few localities have been studied previously. Moreover, previous studies on NAM inclusions in diamonds showed distinct ranges in water concentration between those measured by FTIR spectroscopy and SIMS [3,4], creating a question of whether the techniques can be compared directly. This study aims to expand on the current geochemical database of olivine inclusions in diamonds.

Fluid inclusions in diamonds are thought to be remnants of the diamond forming fluid [5]. Analysis of these fluid inclusions indicate four types of fluid inclusions: saline, silicic, high-Mg carbonatitic and low-Mg carbonatitic. There is a lack of understanding of how the salinity of fluid can change the equilibrium water storage capacity of mantle minerals. Thus, high pressure experiments were conducted to investigate the water concentration of olivine at 2 GPa with fluorine- and chlorine-rich fluids. SIMS was also used to study the variation of the water and halogen concentration in forsterite with respect to the salinity of the fluid in equilibrium with the forsterite. This allows a more accurate quantification of the water and volatile storage capacity of olivine in equilibrium with a saline rich diamond forming fluid.

Samples and method

Lithospheric diamonds from: Argyle, Australia; Diavik, Canada; and Murowa, Zimbabwe, were analysed by SIMS. The samples were previously exposed using a diamond impregnated scaife for FTIR spectroscopy. The surfaces were further polished using 9, 3 and 1 micron polishing pads. The experimental samples were picked individually from four different experimental batches with varying initial fluid composition. The samples were then pressed into indium mounts. Each mount also had a San Carlos olivine pressed into it near the samples. The San Carlos olivine crystals **were used as a "dry"** standard to check the background hydrogen levels for each mount. The mounts were cleaned with ethanol, coated with carbon, placed in the chamber and pumped down for four days as an attempt to minimise the background hydrogen levels.

Results and discussion

Diamond olivine inclusions contain low concentrations of water

Olivine at diamond-forming pressures can store ~ 2000 ppm of water. However, the maximum water

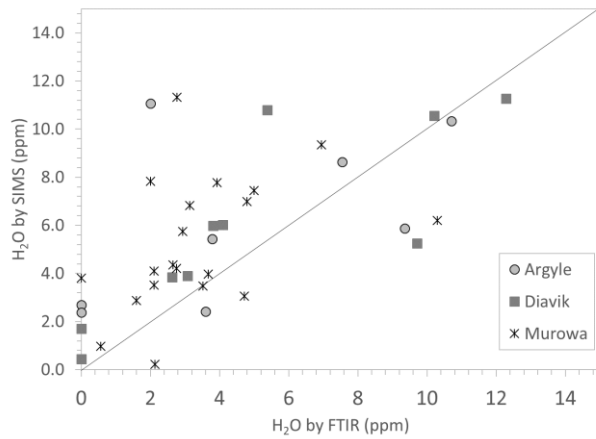


Fig. 1. Comparison of the water concentration obtained by FTIR spectroscopy and SIMS.

analysis via SIMS via whole inclusion analysis via FTIR; approximation of the orientation factor on FTIR calculations and errors in the subtraction method due to noise using FTIR. Nevertheless, this indicates that studies that use one or the other method can be compared.

The water concentrations do not correlate with proxies of enrichment or redox state

The trace element contents indicate a composition that is typical of mantle peridotite, except for the anomalously low phosphorus and lithium concentration. FTIR spectroscopy has shown that water is incorporated into the olivine structure through trace element defects, specifically defects that are associated with fluorine, trivalent cations, titanium and potentially boron. Studies on trace elements in olivine also indicate that Ca, Cu, Li, P and Zn can be used to indicate metasomatism [6]. The V/Sc ratio of olivine has also been used to characterise the redox state. However, the water concentrations do not show any correlation with trace elements.

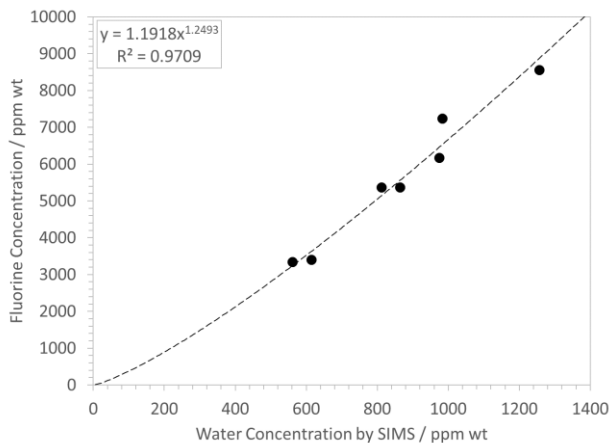


Fig. 2. The variation in the fluorine concentration with the water concentration by weight

concentrations measured were 12.9 ppm in Argyle diamonds, 12.3 ppm in Diavik diamonds and 10.3 in Murowa diamonds. The water concentrations of olivine inclusions in diamonds are similar across all localities, including those from previous studies, suggesting that a similar process may occur that produces relatively dry olivine inclusions.

FTIR spectroscopy and SIMS show comparable water concentrations

Figure 1 shows that FTIR spectroscopy and SIMS produce similar ranges and some correlation in the water concentration. The discrepancies between the two methods include point

Forsterite crystallised in equilibrium with fluoride-containing fluid show a non-linear relationship between fluoride and water concentration.

High pressure solubility experiments show that water concentration increases as the fluorine concentration increases in forsterite. This suggests a coupling between the fluorine and hydroxyl incorporation in olivine. However, the relationship between the fluorine and water concentration is not simple as Fig. 2 suggests, because FTIR data show that as the fluorine to water ratio increases, defects with more fluorine replacing the oxygens around a silicon vacancy become more stable.

References

[1] Stachel T et al. (2005) Elements 1, 73-78; [2] Shirey SB et al. (2011) Science 333, 434-436; [3] Novella D et al. (2015) Lithos 230, 180-183; [4] Taylor LA et al. (2016) EPSL 433, 125-132; [5] Navon O et al. (1988) Nature 335, 784; [6] De Hoog JCM et al. (2010) Chemical Geology 270, 196-215.

Sulfur isotopic evidence for a volatile-enriched recycled component in the Canary Islands mantle source

Z. Taracsák¹, M.E. Hartley¹, D.A. Neave^{1,2}, M. Edmonds³, A. Turchyn³, M-A. Longpré⁴, R. Burgess¹

¹Department of Earth Sciences, University of Manchester, Manchester M13 9PL, UK

²Institut für Mineralogie, Universität Hannover, Callinstrasse 330167 Hannover, Germany

³Department of Earth Sciences, University of Cambridge, Cambridge CB2 3EQ, UK

⁴School of Earth and Environmental Sciences, Queens College, City University of New York, NY 11367, USA

Background and Motivation

El Hierro is located in the westernmost part of the Canary Islands, 500 km west of the coast of Africa. A submarine eruption in 2011-2012 along the southern rift arm of El Hierro was fed by one of the most sulfur-enriched magmas compared to other ocean islands worldwide, with melt inclusions containing up to 5000 ppm S [1]. The sulfur- and CO₂-rich nature of El Hierro magmas is now well documented for past eruptions [2]. Melt inclusion (MI) volatile and trace element contents indicate El Hierro magmas might have formed from a sulfur-enriched mantle source containing both recycled crustal and asthenospheric mantle sulfur [2]. However, previous studies have been ambiguous whether S enrichment is related to low mantle melting degree or the presence of recycled S in a metasomatised mantle source. We measured sulfur isotopes in a suite of olivine-hosted MIs from El Hierro, and use the data to evaluate if recycled S is present in the mantle source. Sulfur isotopes are a powerful tool for tracing recycled S in the mantle source of ocean island basalts because they are strongly fractionated by surface processes in reservoirs **such as seawater** ($\delta^{34}\text{S} \sim 20\text{‰}$) or sediments containing biogenic sulfide ($\delta^{34}\text{S}$ to -30‰) compared to ambient upper mantle ($\delta^{34}\text{S} = -0.9\text{‰}$). If recycled S is present in the El Hierro mantle source, $\delta^{34}\text{S}$ of primitive magmas will differ from ambient mantle value. Furthermore, correlation **between** $\delta^{34}\text{S}$ and trace element enrichment of melts indicated by a high La/Yb ratio would directly link recycled S to a subducted slab in the mantle source.

Results

We analysed 75 glassy MIs and matrix glasses from rapidly quenched tephra samples from El Hierro for ³⁴S/³²S ratios and sulfur content at EIMF using the CAMECA IMS-1270. Twenty-five inclusions were previously analysed for trace elements by SIMS in 2017 (IMF 600/1016), providing an opportunity to evaluate directly if there are any links between trace element enrichment and melt $\delta^{34}\text{S}$.

The sulfur isotopic compositions of El Hierro melt inclusions strongly correlate with S content (Fig. 1), indicating extensive S isotope fractionation during sulfur degassing. The fractionation factor, determined using a logarithmic fit to our data, is 1.006 ± 0.001 , suggesting that degassing of SO_{2(gas)} occurred from a melt containing both S²⁻_(melt) and SO₄²⁻_(melt) [3]. By analysing a set of melt inclusions with variable S contents, the pre-**degassed** $\delta^{34}\text{S}$ of the melt can be traced back to its original value, providing an opportunity to evaluate the sulfur isotopic composition of the primary melt.

El Hierro melt inclusions are highly variable in terms of their incompatible trace element ratios, such as La/Yb [2]. Samples with different La/Yb can thus provide insight on the S-isotopic composition of variably enriched mantle source components. We divided our samples into two main groups: melt inclusions with high La/Yb (La/Yb_{avg} > 20) and low La/Yb (La/Yb_{avg} < 20), which represent the highly-enriched and less-enriched end-members of El Hierro melts (Fig. 1). Our results indicate that melts from low La/Yb samples originally contained ~3500 ppm S with an isotopic composition close to $0 \pm 0.5 \text{‰}$, which **overlaps with most recent** $\delta^{34}\text{S}$ estimates for the depleted mid-ocean ridge mantle. **High La/Yb samples from El Hierro have around 4500 ppm S and an undegassed** $\delta^{34}\text{S}$ of $3 \pm 0.5 \text{‰}$, which is outside the limits of published **mantle estimates**. **Positive** $\delta^{34}\text{S}$ compared to mantle values indicates that trace element-enriched melts from El Hierro contain sulfur that was isotopically fractionated by surface processes, in this case most likely seawater alteration, then recycled into the mantle during slab subduction. Low La/Yb melt inclusions, on the other hand, only contain ambient mantle sulfur, pointing to a primitive mantle source. Positive primary melt $\delta^{34}\text{S}$ of $3 \pm 0.5 \text{‰}$ observed in trace element-enriched

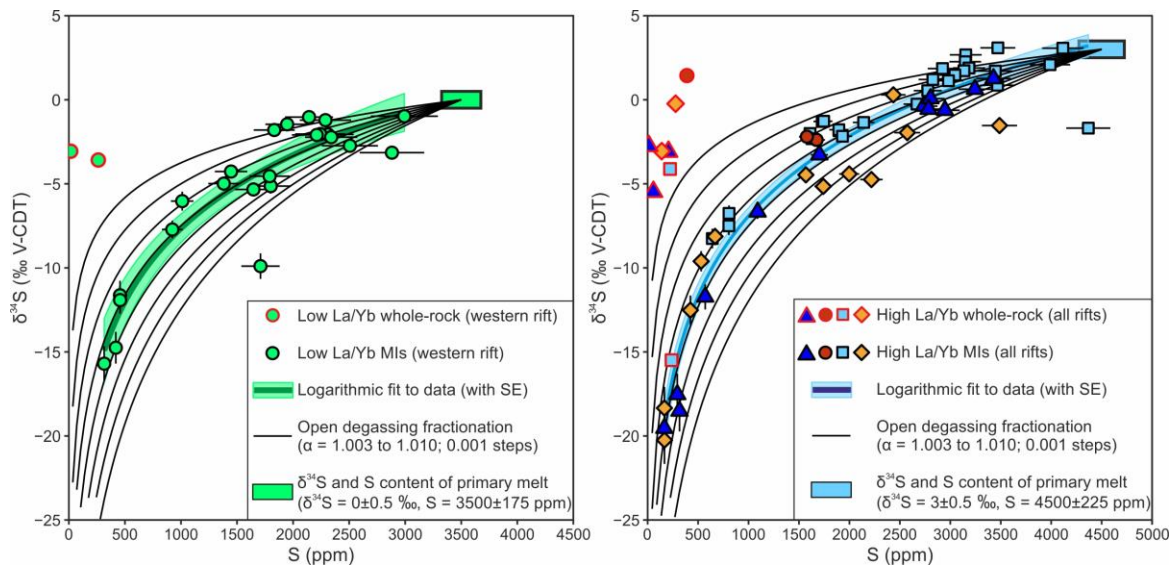


Figure 1. Sulfur isotopic composition of low (left, samples from Montaña Negra, western rift of El Hierro) and high (right) La/Yb melt inclusions and whole-rock samples from El Hierro. Black lines indicate degassing pathways. Coloured curves are logarithmic fits to the melt inclusion data, with fields around them indicating 1 standard error of the fit parameters. Coloured boxes indicate primary magma $\delta^{34}\text{S}$ as S content based on the data and the logarithmic fit.

samples can be explained by mixing 20 % seawater-derived sulfur ($\delta^{34}\text{S} = 20.3\text{‰}$) with 80% mantle S with $\delta^{34}\text{S}$ of -0.9‰ .

Our results provide a direct link between previously subducted slabs in the mantle source of ocean island basalts, identified based on trace element enrichment of melts, and sulfur enrichment in the melt. This suggests that a significant portion of sulfur found in subducting slabs survives devolatilisation during slab dehydration and is recycled into the mantle. This sulfur likely ends up in parts of the mantle which interacts with the remnants of the slab, producing a mantle that is heterogeneous in terms of S and possibly other recycled volatiles even on short length scales such as the mantle source feeding eruptions at a small ocean island like El Hierro.

Appendix

During the project we also carried out the first systematic investigation of instrumental mass fractionation (IMF) effects on sulfur isotope ratios during SIMS analyses. We analysed nine glass standards with known bulk $\delta^{34}\text{S}$ composition, variable major element composition (picrite to rhyolite) and sulfur content (500-3500 ppm) in three sessions. We found matrix effects up to 12 ‰ between different glasses (Fig. 2). The value of the IMF does not correlate strongly with any major elements, but does correlate with sulfur content (Fig. 2). Our ongoing work seeks to understand the cause of this correlation.

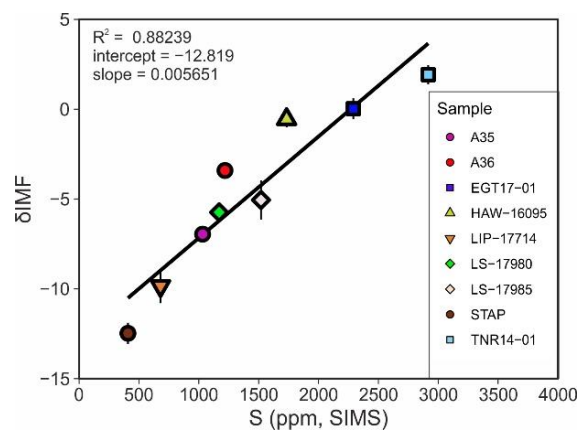


Figure 2. Instrumental mass fractionation values (relative to EGT17-01) of standard glasses with known $^{34}\text{S}/^{32}\text{S}$ ratio vs. S content. Data is from session 9 on 25/11/2019

References

- [1] Longpré et al. (2017) Earth and Planetary Science Letters, 460, 268-280.
- [2] Taracsák et al. (2019) Geochimica et Cosmochimica Acta, 258, 19-36.
- [3] Marini et al. (2011) Reviews in Mineralogy & Geochemistry, 73, 423-492.

Deep volatile cycling and terrestrial thermal evolution

C. Walton¹, N. Potts², E. Mare³, I. Buisman¹, G. Bromiley², S. Mikhail³

¹Department of Earth Sciences, University of Cambridge, Cambridge CB2 3EQ

²School of GeoSciences, University of Edinburgh, Edinburgh EH9 3JW, UK

³School of Earth & Environmental, University of St. Andrews, St. Andrews KY16 9AL, UK

Aim of the pilot study

Quantifying the mechanics of heat-producing element distribution (e.g. ⁴⁰K) in Earth over time is required **to develop models for Earth's temporal development**. Heat flow controls planetary cooling rate and thermal structure, which in turn determines the dominant geodynamic regime (e.g. subduction zone plate tectonics on Earth). Mantle ⁴⁰K⁺ is largely hosted in pyroxene at low concentrations (<100 ppm, e.g. [1]). Our pilot project aimed to determine the influence of negatively-charged volatiles (OH⁻, Cl⁻) on pyroxene-melt K⁺ partitioning under P-T conditions consistent with **Earth's upper mantle**, in order to test links between deep volatile cycling and the re-distribution of heat flow over Earth history.

Results

We measured K abundance in pyroxene and silicate melt phases present in four of our experimental runs. These experiments were conducted in the system pyroxene–silicate melt under P-T conditions akin to the upper mantle, with variable volatile contents (e.g. H₂O, Cl). The K data obtained via Secondary Ionisation Mass Spectrometry (SIMS) on the Cameca IMS 7f-Geo instrument are plotted in Fig. 1 as pyroxene-melt Nernst partition coefficients (D values), along with major element exchange coefficients (K_D values) for Mg=Ca, measured separately by EPMA.

Outcome

Fig. 1 shows that K partitioning behaviour is not notably affected by the presence of Cl, OH, or Cl + OH in the melt. We have observed statistically significant correlations between volatile element content and the partitioning behaviour of other cationic species with (e.g., Ca and Mg mineral-melt exchange, in Fig. 1). In the case of K, however, any such variation in behaviour falls within the bounds of analytical error. An exception is Run Cl + OH. This experiment contains both clinopyroxene and orthopyroxene, but we were unable to measure K in the latter phase. K is notably low in opx identified in our other multi-pyroxene bearing experimental run (Cl), indicating that there is no observable change in K behaviour in any of these experimental samples. Our results indicate the following: [1] K⁺ is similarly incompatible in pyroxene at arc mantle conditions across melt K concentration ranges of 10000-100s of ppm (i.e., when comparing to Chamorro et al., 2002) and that [2] unlike divalent major elements such as Ca and Mg, K min-melt partitioning behaviour can be modelled as essentially insensitive to Cl and OH abundances(s). These valuable results remove uncertainty from our understanding of both K-induced heat production, and K⁺-NH₄⁺ exchange (Zerkle & Mikhail, 2017) in the deep Earth. Our results will be submitted as a journal article later this year.

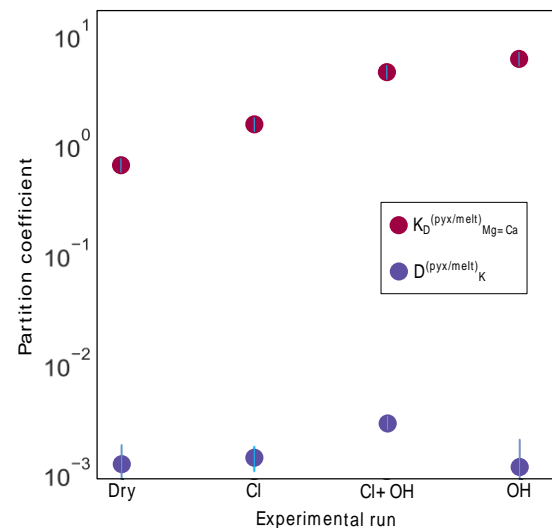


Figure 1. Pyroxene-melt partition coefficients. The values given are exchange or K_D values in the case of Mg=Ca exchange and Nernst partition coefficients or D values in the case of K. Where possible, weighted partition coefficients accounting for the relative abundances of both clino- and ortho-pyroxene in an experimental run have been calculated.

References: [1] E.M. Chamorro et al. (2002) GCA 66, 507-519, [2] A.L. Zerkle and S. Mikhail (2017) Geobiology 15, 343-352

Is Early Earth bombardment history recorded in shocked meteorites?

C. Walton¹, O. Shorttle¹ & M. Anand²

¹Department of Earth Sciences, University of Cambridge, Cambridge CB2 3EQ

²Department of Physical Sciences, Open University, Milton Keynes, MK7 6AA

Aim of the pilot study

Meteorites provide evidence to test models of **Earth's** early bombardment history, through their own record of high-energy collisions recorded in reset apatite U-Pb ages. Clustered age distributions would constrain periods of enhanced collisional activity across the inner Solar System [1]. We aimed to establish whether or not there was sufficient U and Pb in phosphate mineral grains from our sample suite of shocked meteorites (Fig. 1) to achieve at least 60 Myr 2σ age uncertainties.

Results

Fig. 2 presents U data collected using the Cameca 7f-Geo during our 1-day pilot study. Literature values for U abundance measured during SIMS analysis of shocked chondritic apatite are also plotted. From Fig. 2, it is clear that the U contents observed in our samples are quite typical in the context of published works. The final reported U-Pb age uncertainties determined in previous apatite U-Pb SIMS studies are plotted in Fig. 2. Two-sigma age uncertainties for U abundances in the 1-5 ppm range (overlapping the vast majority of results obtained in our pilot study) are invariably less than 60 Myr.

Outcome

On the basis of the data obtained, we concluded that (1) our samples were comparable with many chondritic apatites previously analysed via SIMS for U-Pb (2) that the < 60 Myr (2σ) final age uncertainty goal set out in our initial application should be achievable for the sample set in question. We prepared and submitted a full application for time on the Cameca 1270, which was ultimately rejected on the basis of the estimates of error calculated by the steering committee (± 120 Myr, 2σ). We intend to apply to EIMF in the future, revisiting the error analysis for U-Pb dating in apatites.

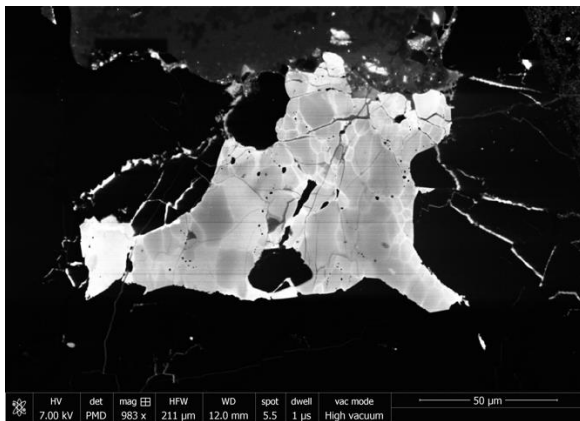


Figure 1: Representative shock recrystallised phosphate (Chelyabinsk, LL5).

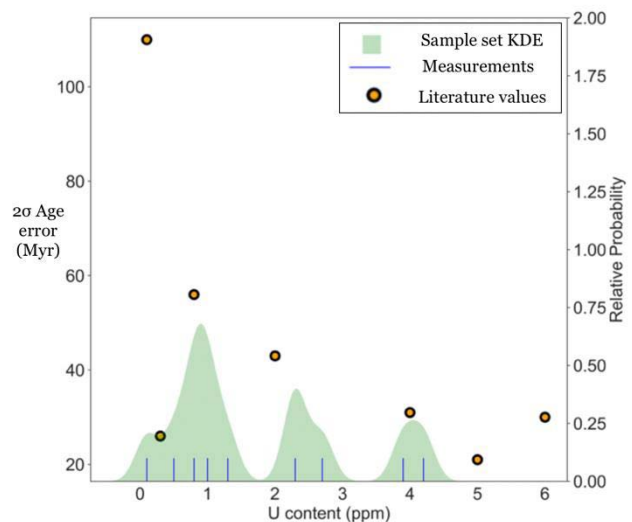


Figure 2: U content of shocked apatite measured in this pilot study vs. U content and 2σ age uncertainties of representative shocked apatite SIMS studies selected from the published literature.

References

[1] W. E. Bottke (2015) Science 348

Trace element compositions of Snæfellsjökull, Oræfajökull and Miðfell volcanic centres, Iceland

E. Waters¹, M. Hartley¹, R. Burgess¹, A. Pawley¹, S. Halldorsson² & O. Shorttle³

¹Department of Earth and Environmental Science, University of Manchester, Manchester, M13 9PL, UK

²NordVulk, Institute of Earth Sciences, University of Iceland, 101 Reykjavik, Iceland

³Department of Earth Sciences, University of Cambridge, Cambridge, CB2 3EQ, UK

Background and objectives

Melt inclusions trapped in early-crystallising minerals can preserve the variable compositions of primary melts supplied to Icelandic volcanic systems, which are subsequently lost from the whole-rock record due to concurrent mixing and crystallisation [1-3]. Melt inclusions can therefore be used to trace differing melt compositions supplied to volcanic systems and magmatic histories prior to eruption. We have analysed suites of olivine- and plagioclase-hosted melt inclusions from Miðfell in Iceland's Western Volcanic Zone, and Snæfellsjökull and Oræfajökull, volcanic centres in the flank zones out-with the active neovolcanic rifts. Miðfell erupts tholeiitic melts from both MORB-like and primordial mantle sources. The flank zones sample small-volume enriched alkali basaltic melts. We measured trace elements and REEs to investigate the heterogeneity of melts supplied to the different localities and differences between rift zone vs flank zones.

Results

Approximately 50 inclusions were measured from both Miðfell and Snæfellsjökull and 6 inclusions measured from Oræfajökull. Miðfell melt inclusions show the greatest variability, displaying both depleted and moderately enriched LREE trends (Fig. 1). Both flank zones show enriched trace element concentrations, with Snæfellsjökull showing the greatest enrichment in LREEs. Melt inclusion suites from the rift zones typically display greater heterogeneity than those from the flank zones. The reason for lack of variability in the flanks is still an open question. It is possible that the small melt fractions sample a limited range of mantle lithologies and/or a less heterogeneous mantle. Alternatively, more extensive melt mixing could have masked any original heterogeneity in the parental melts.

Depleted inclusions from Miðfell have the lowest La/Sm values (Fig. 2), consistent with high degrees of melting of a mantle source similar to depleted MORB mantle. **Miðfell's** enriched population has higher La/Sm similar to inclusions from Oræfajökull. These higher La/Sm inclusions have generally greater Sm/Yb, indicating that they sample smaller degree melts from a more enriched mantle domain.

The trace element systematics suggest that this enriched domain is common to both Miðfell and Oræfajökull. Snæfellsjökull melt inclusions sample both the smallest degree and most enriched melts. To investigate differences in the flank zone compositions, we compare their trace element systematics to global OIB samples (Fig. 3). HIMU sources define a relatively constrained region in Sr/Nb vs. Ba/Nb space. EM1 and EM2 are more variable due to differences in the recycled sedimentary component influencing individual mantle domains [4]. Snæfellsjökull appears to display an EM-like signature approaching the HIMU field. Oræfajökull does not

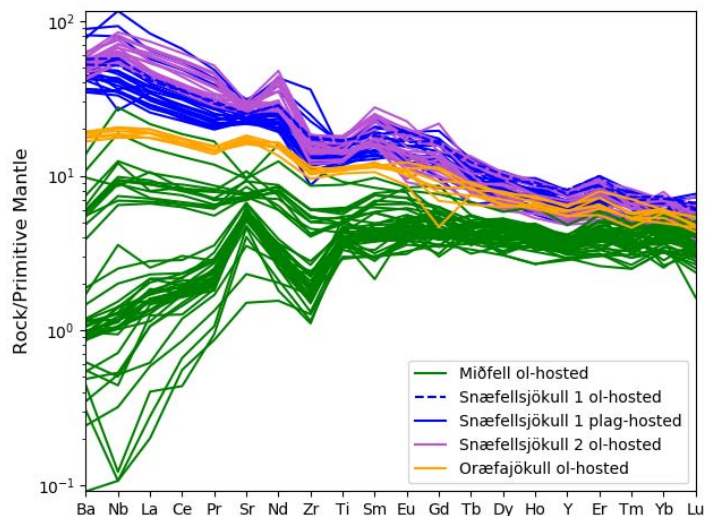


Figure 1 - Trace element abundances of volcanic centres normalised to primitive mantle values

overlap with global EM signatures, although we note that the range of possible EM-derived melt compositions is expected to be high. Our data suggest that there are intrinsic differences in the compositions of melts from the two flank zones, reflecting lithological heterogeneity in their source regions.

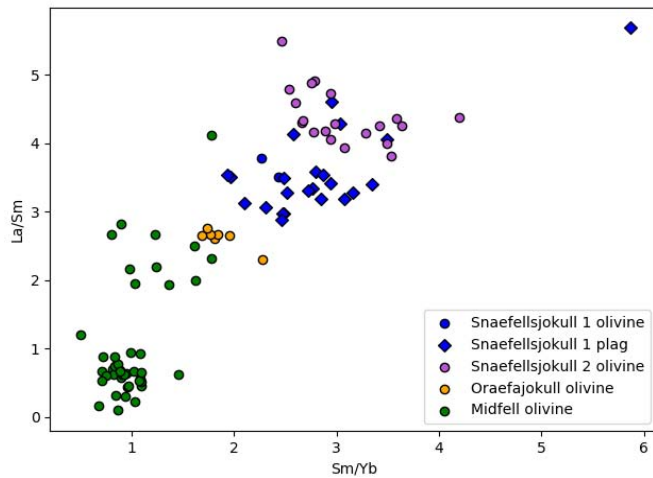


Figure 2 - Sm/Yb vs La/Sm for melt inclusions. Higher La/Sm indicates lower degrees of melting. Higher Sm/Yb greater enrichment of the melt.

Greater involvement of recycled sediment in the source of Oraefajökull melts may account for their higher Sr/Nb compared to Snæfellsjökull.

While there is little heterogeneity within melt inclusions from our two Snæfellsjökull samples, we observe systematic differences in trace element ratios between the samples (Fig. 2, Fig. 3). The sample locations are ~10 km apart. Both were erupted during the last glacial period (700-10 ka), although precise eruption ages are not known. It is possible that the higher La/Sm ratios could have been produced by higher melting degrees in the shallow mantle towards the end of the last glacial period, in response to ice unloading [5].

Ongoing and future work

Current work focuses on using our new trace element data to investigate the causes of limited heterogeneity within flank zone melt inclusions compared to those from neovolcanic zones; the mantle source lithologies supplying melts to the flank zones; and how the proportions of recycled material within the mantle might vary across Iceland. Future work will investigate the halogen concentrations of different mantle sources in Iceland to trace recycled crustal material in these domains. We have already measured F and Cl, and we plan to measure Br and I in the same melt inclusions later in 2020.

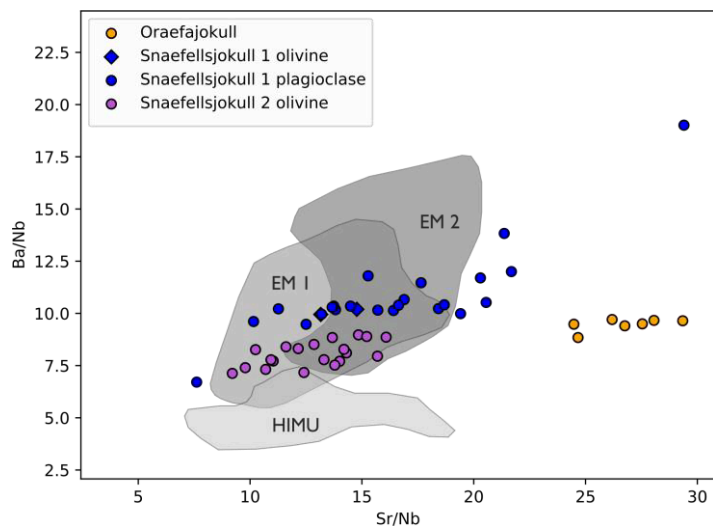


Figure 3 - Sr/Nb vs Ba/Nb of melt inclusion compared to global OIB measurements. HIMU and EM database [4].

References

- [1] J. Maclennan et al. (2003) *Journal of Geophysical Research* 108
- [2] M. E. Hartley et al. (2015) *Earth and Planetary Science Letters* 425, 168-178
- [3] J. Maclennan (2008) *Geochimica et Cosmochimica Acta* 72, 4159-4176
- [4] M. Willbold and A. Stracke (2006) *Geochemistry, Geophysics, Geosystems* 7(4).
- [5] B. Hardarson and J. Fitton (1991) *Nature* 353, 62-64

Petrological insights into the volatile budget of the 2018 Kīlauean eruption

P. E. Wieser¹, H. Lamadrid², M. Edmonds¹, J. Maclennan¹, F.E. Jenner³

¹ Department of Earth Sciences, University of Cambridge, UK. pew26@cam.ac.uk

² Geological Sciences, University of Missouri, 65211, US

³School of Environment, Earth and Ecosystem Sciences, The Open University, MK7 6AA, UK

Background and rationale

The 2018 eruption marked the most significant change in eruptive character at Kīlauea Volcano in the last 35 years, terminating the long-lived Pu'ū 'Ō'ō eruption. Twenty four separate fissures opened in the Lower East Rift Zone between the 3rd and 27th of May, with activity localizing at Fissure 8 (F8) by the end of May¹. The early fissures tapped relatively evolved, rift-stored magmas. Throughout May, glass and crystal compositions became increasingly primitive, as summit-derived magma flushed out the rift-zone storage reservoirs. These progressive changes in chemistry were interrupted by relatively explosive outbursts of highly evolved andesitic lava from F17². Constraining the volatile budget of this eruption is vital for two reasons. Firstly, the co-eruptive emissions of SO₂ were unprecedented, causing significant perturbations in regional air quality³. Secondly, the lava erupted from the early fissures are among the most differentiated samples ever collected at Kīlauea, providing novel constraints on the evolution of volatiles during fractional crystallization at ocean island volcanoes.

Results and discussion

We performed in-situ analyses of ~350 olivine-, pyroxene- and plagioclase-hosted melt inclusions and co-erupted matrix glasses by SIMS (H₂O, CO₂, F), Raman spectroscopy (vapour bubble CO₂), EPMA (major elements, Cl, S), and LA-ICP-MS (~60 lithophile and chalcophile elements). Our samples incorporate differentiated rift-stored basalts from early May (MgO_{glass}=3.6–4.9 wt%), a time series of the activity at F8 (May 7th to August 1st, MgO_{glass}=5.9–6.7 wt%), as well as the extremely differentiated compositions erupted at F17. In contrast to whole-rock data², our glass measurements classify this composition as dacitic (MgO_{glass}=1 wt%, SiO_{2, glass}=65 wt%, Na₂O+K₂O=6 wt%).

Olivine-hosted melt inclusions from F8 lavas between June and August have experienced large quantities of post-entrapment crystallization (PEC; up to 35%), due to the entrainment of highly primitive olivine crystals (up to Fo₈₉) into carrier liquids with ~6–7 wt% MgO. Changes in major element chemistry during extensive PEC combined with the incompatible behaviour of CO₂ drive the formation of a CO₂-rich vapour bubble⁴. Raman spectroscopy reveals that F8 vapour bubbles contain ~40–99% of the total melt inclusion CO₂ (Fig. 1). Melt CO₂ contents measured using SIMS give barometric estimates of a few hundred metres, while CO₂ contents estimated by combining Raman and SIMS data yield

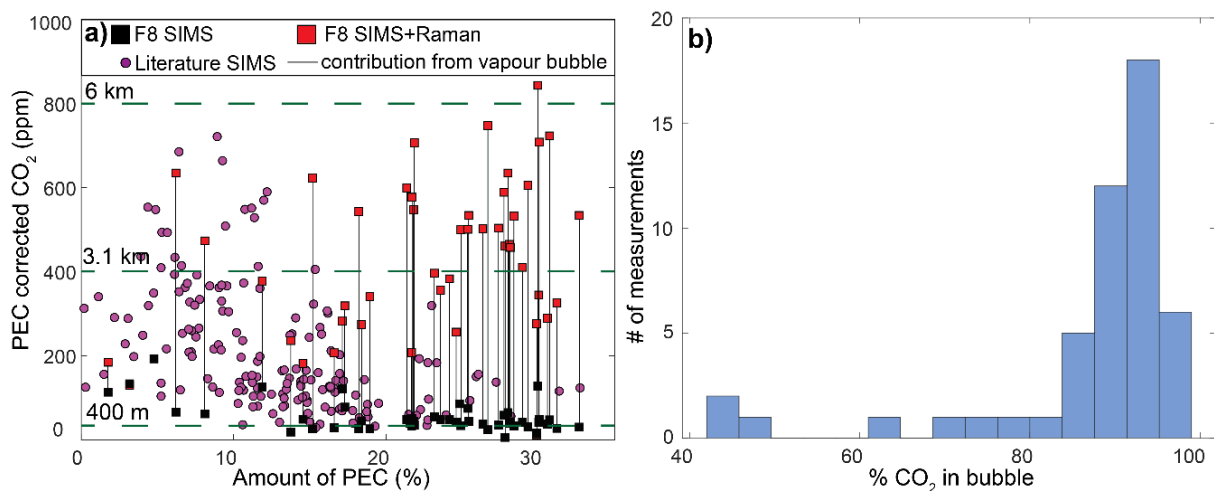


Figure 1. Significant quantities of the total carbon budget of F8 melt inclusions are held in vapour bubbles.

magma storage depths between ~2–6 km (aligning with geophysical datasets; Fig. 1). In contrast, olivine-, pyroxene- and plagioclase-hosted melt inclusions from early rift-stored lavas have experienced limited PEC, and have no quantifiable CO₂ in vapour bubbles. Their CO₂ contents range from ~0–500 ppm, indicative of rift-zone storage at ~3 km.

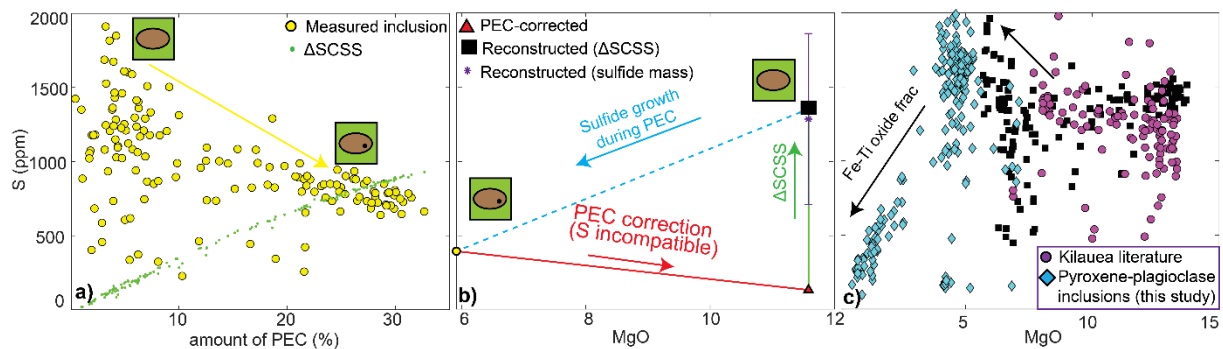


Figure 2. a) Melt inclusions show a strong correlation between S contents and the amount of PEC. b) Initial melt S contents were reconstructed by calculating the change in the SCSS during PEC, and by measuring visible sulfides. c) Reconstructed S contents align with literature data⁵.

There is an inverse correlation between melt inclusion S concentrations and the amount of PEC in F8 samples (Fig. 2a). We attribute this to sulfide saturation following melt inclusion entrapment, driven by Fe-loss associated with PEC. This causes up to 1000 ppm S to be sequestered within small sulfides. Initial melt S contents were reconstructed by adding the change in sulfide solubility (the SCSS) associated with major element changes during PEC to measured melt inclusion S contents. These reconstructed values overlap with estimates where the loss of S was estimated by measuring the volume of sulfides within melt inclusions (Fig. 2b). As reconstructed S contents approximately align with literature data for **Kīlauean** eruptions that have experienced considerably less PEC⁵, high atmospheric fluxes of S were likely caused by high effusion rates, rather than anomalously S-rich melts. More evolved rift-stored melt inclusions show an increase in S contents between ~7 and 4 wt% MgO (during concurrent ol-px-plag fractionation), and a drastic drop between ~4 and 1 wt% MgO (following Fe-Ti oxide fractionation; Fig. 2c). This drop in S is accompanied by a rapid drop in Cu, and a substantial increase in the number of sulfides in erupted products.

Melt inclusion Cl and H₂O behave incompatibly with progressive differentiation, resulting in the F17 dacite having the highest melt Cl (~1000 ppm) and H₂O concentrations (~2 wt%) ever reported for erupted **Kīlauean** lavas (Fig. 3). F also behaves incompatibly until the onset of apatite saturation at ~2.5 wt% MgO. Overall, we demonstrate that extensive differentiation of an initially volatile-poor basalt at relatively shallow depths can generate very H₂O and Cl-rich, but S-poor melts.

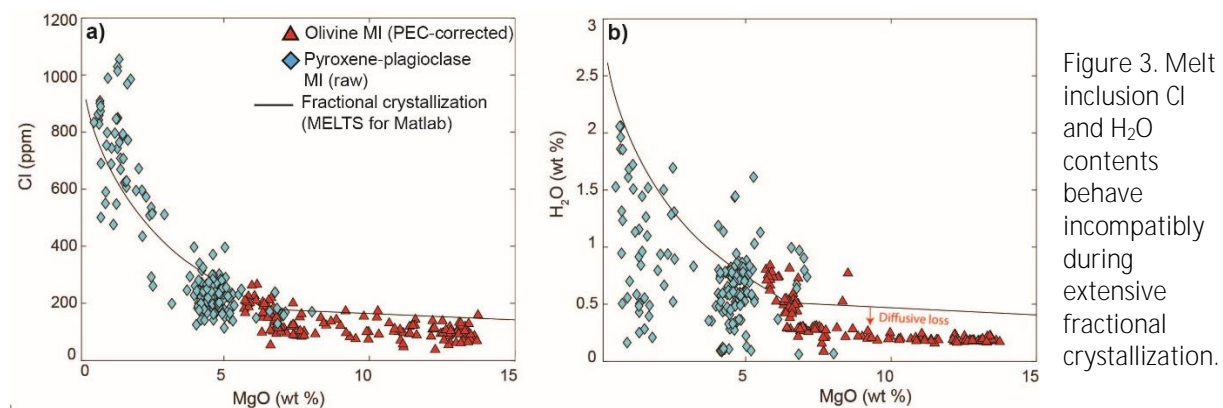


Figure 3. Melt inclusion Cl and H₂O contents behave incompatibly during extensive fractional crystallization.

References

- [1] https://volcanoes.usgs.gov/vsc/file_mgr/file-179/Chronology%20of%20events%202018.pdf; [2] Gansecki et al. (2019) Science 366, 10.1126/science.aaz1822; [3] Whitty et al. (2020) Frontiers 10.3389/feart.2020.00036; [4] Maclennan (2017) G³ 18, 597-616; [5] Wieser et al., in review. <https://eartharxiv.org/u6j79>